CHARACTERIZATION OF NON-FARADAIC LABEL FREE IMPEDIMETRIC ELECTROCHEMICAL SENSOR

by

Nurcan GÜNGÖRDÜ

B.Sc. Bioengineering, Metallurgy and Chemistry Faculty, Yildiz Technical University, 2015

Submitted to the Institute of Biomedical Engineering
in partial fulfillment of the requirements
for the degree of
Master of Science
in
Biomedical Engineering

Boğaziçi University
2018

ACKNOWLEDGMENTS

It's been a very long road for me to complete this journey, but here I am at the end, but there are so many people to whom thanks I extend!

I would like to thank to my advisors, Professor Şenol Mutlu and Assist. Prof. Dr. Bora Garipcan. Bora Garipcan is someone you will instantly admire and never forget once you meet him if we think about Biomedical Engineering Institute. He is an enthusiastic and energetic advisor and tries to help every topic that he can. I thank to him to give me the chance to make my thesis on an integrated area and meet me one of the hardest and also excited scientist in University as being my co-advisor with Şenol Mutlu who has always been supportive for my research. He has also provided insightful discussions about the research. I am also very grateful to him for his scientific advice and knowledge and many insightful discussions and suggestions. He is my primary resource for getting my science questions answered and was instrumental in helping me cranked out this thesis. Dear Professor Şenol, thank you for accepting me and widen my envision for this area. Your knowledge is like mountains. I am very lucky to have this thesis with you and your team.

Doors to their office were always open whenever I ran into a trouble spot or had a question about my research or writing.

I am indebted to my many friends for providing a stimulating and fun environment in which to learn and grow. First of all I would like to begin my gratitude to my laboratory friends. I couldn't finish this project without MEMS laboratory members: Ozan Ertop, Gürkan Sönmez, Kemal Ünlü, Kerem and my only woman soul-mate Sinem Orbay. I deeply thank to Ozan who have still been answered my huge amount of inquiries kindly even they are silly questions, Kemal is the coolest one our laboratory and everyone knows what I mean in the lab, Gürkan is a father of our lab regarding his smartness, experiences and style, and Sinem who is still supporting and listening

me; Sinem I am very glad to meet you and sharing our lunch together was a honour for me. I spent very valuable, funny time besides science and academic. I hope every one of you would catch your dreams in someday.

Finally, I must express my very profound gratitude to my parents and to my boyfriend (Oh my God! He is my fiance now) for providing me with unfailing support and continuous encouragement throughout my years of study and through the process of researching and writing this thesis even they haven't understand even a single word. This accomplishment would not have been possible without them. I hope this end will bring new beginnings.

Thank you God! for giving me that strength to accomplish many challenges in my life as this is, I know I will continue to fight for my life as I live. So, adventures in my life would be easier if I have that kind of people around me.

Thanks again,

Nurcan Güngördü

ACADEMIC ETHICS AND INTEGRITY STATEMENT

I, Nurcan GÜNGÖRDÜ, hereby certify that I am aware of the Academic Ethics and Integrity Policy issued by the Council of Higher Education (YÖK) and I fully acknowledge all the consequences due to its violation by plagiarism or any other way.

Name :

Signature:

Date:

ABSTRACT

CHARACTERIZATION OF NON-FARADAIC LABEL FREE IMPEDIMETRIC ELECTROCHEMICAL SENSOR

The developments in microfluidics and BioMEMS have led to miniaturized high-performance droplet-based sensors. These sensors must be reliable, simple, fast-responding and cost-effective to be used in biomedical applications. In this work, the non-faradaic electrochemical impedimetric approach is studied to measure different salt concentrations and different pH values. Label-free measurements are done to characterize electrical double layer capacitance (Cedl) and solution resistivity (Rs). For this purpose, gold interdigitated electrode (AuIDE) is fabricated on a glass wafer. Three different salt (LiCl, KCl and NaCl) solutions in different molarities between 0,001M to 0,1M and with different pH values (pH range between 2.0 to 11.50 at constant conductivity) are prepared. Impedance measurements are taken from an AuIDE at a frequency range of 20 Hz to 10 MHz, with an amplitude of 10 mV using an Impedance Analyzer (E4990A) to extract the values of Cedl and Rs. The data is interpreted according to both Cedl and Rs values and Nyquist plots. Results for both salt and pH solutions exhibit that as solution molarity increases, the Cedl values also increases and each solution shows different patterns on Nyquist plots. This study can lead to label free measurement of analyte type, concentration and pH values upon data processing of multiple reference and analyte measurements.

Keywords: Electrical double layer, impedimetric sensor, salt concentration and pH characterization, Nyquist plots, data processing.

ÖZET

ETİKETSİZ FARADAİK OLMAYAN İMPEDİMETRİK ELEKTROKİMYASAL SENSOR KARAKTERİZASYONU

Mikroakışkanlar ve BioMEMS'deki gelişmeler minyatürize yüksek performanslı ve damlacık tabanlı sensörlerin çalışılmasına olanak sağlamıştır. Bu sensörler biyomedikal uygulamalarda kullanılmak üzere hızlı yanıt veren, güvenilir, basit ve düşük maliyetli olmalıdır. Bu çalışmada, faradaik olmayan elektrokimyasal impedimetrik yaklaşım farklı tuz konsantrasyonlarını ve farklı pH değerlerini ölçmek için kullanılmıştır. Etiketsiz ölçümler, solüsyondaki elektriksel çift tabakanın kapasitansını (Cedl) ve solüsyonun direncini (Rs) karakterize etmek için yapılmıştır. Bu amaçla, cam ara tabakasında altın interdijite elektrot (AuIDE) fabrike edilmiştir. 0,001M ve 0,1M arasındaki farklı molaritelerde üç farklı tuz (LiCl, KCl ve NaCl) ve sabit iletkenlikte 2.0 ve 11.50 arasında farklı pH solüsyonları hazırlanmıştır. Empedans ölçümleri, Cedl ve Rs değerlerini elde etmek için Empedans Analizörü (E4990A) kullanılarak 20 Hz ila 10 MHz frekans aralığında ve 10 mV'lik bir amplitüd ile interdijite altın elektorde yüzeyine solüsyon damlatılarak alınmıştır. Veriler, her bir solüsyon için Cedl ve Rs değerlerine ve Nyquist grafiklerine göre yorumlanmıştır. Hem tuz hem de pH çözeltilerinin sonuçları doğrultusunda, molaritenin artmasıyla, Cedl değerlerinin arttığını ve her bir solüsyonun Nyquist grafikleri üzerinde farklı rejimler sergilediğini göstermektedir. Bu çalışma veri analizi, çoklu referans ve analit ölçümlerinde analit tipi, konsantrasyon ve pH değerlerinin etiketsiz ölçümüne farklı bir bakış açısı sunmaktadır.

Anahtar Sözcükler: Elektriksel çift tabaka, impedimetrik sensor, tuz konsantrasyonu ve pH karakterizasyonu, Nyquist grafiği, data proses.

TABLE OF CONTENTS

LIST OF FIGURES

LIST OF TABLES

LIST OF SYMBOLS

Z	Impedance
Z'	Real part of impedance
Z''	Imaginary part of impedance
Z_m	Measured impedance
C_{edl}	Electrical double layer capacitance
R_{sol}	Solution resistance
C_{sol}	Solution capacitance
M	Molar
F	Farads
Hz	Hertz
C	Capacitance
V	Voltage
L	Liter
q	The charge unit
k	the Boltzmann's constant
T	Temperature
C_H	Stern layer
C_D	Diffuse layer
R	Resistance
X	Reactance
Q	Constant phase element coefficient
α	Exponent of constant phase element
μ	Micro
Ω	Ohm
ω	Angular frequency
σ	Charge density
Ψ	Inner potential
ε	Dielectric constant

ε_0	Air permittivity
θ	Phase angle

LIST OF ABBREVIATIONS

AC	Alternative Current
AuIDE	Gold Interdigitated Electrode
BioMEMS	Biomedical Microelectromechanical Systems
CPE	Constant Phase Element
DC	Direct Current
EDL	Electrical Double Layer
GERD	Gastroesophegeal Reflux Disease
IC	Interdigitated Circuits
IDE	Interdigitated Electrode
IHP	Inner Helmholtz Plane
IPE	Ideal Polarizable Electrode
LOC	Lab-on-a-Chip
MEMS	Microelectromechanical Systems
OHP	Outer Helmholtz Plane
POC	Point of Care
Pr	Photoresist
PZC	Point of Zero Charge
UV	Ultraviolet
VLIC	Very Large Scale Interdigitated Circuits

1. INTRODUCTION

The increasing population of human has given rise to expanding demand for hospitals, physicians, and point of care (POC) technologies [1], which, in turn, increased health care cost. This resulted in a need for low cost, fast and high throughput diagnosis tools. The burden of these necessities doubles with the need for accurate detection of molecules and ions for a wide variety of diseases [1]. For this purpose, microdevices have been developed especially for POC. They promise cheap, rapid and portable solutions [2]. The advancement of microdevice diagnostics was originated from microelectronics revolution, which contributed to miniaturization and integration of semiconductor devices and their microfabrication processes [2]. These advancements initially led to integrated circuits (IC) and later to very large scale integrated (VLSI) circuits.

After the success of IC concept, microfabrication techniques have been broadened with bulk and surface micromachining of silicon and glass. This led to a new research area called micro-electro-mechanical systems (MEMS). These research efforts used thin films and bulk of many variety of materials ranging from diamond, SiC, gold to plastics and polymers. Later, this area was further broadened by a set of microfluidic mechanical devices and systems. This new area was called as microfluidics and lab-on-a-chip (LOC) systems [2]. One of the main application area of these developments has always been biomedical field. A broad range of sensors especially in biomedical technology and science has been developed in the light of these microdevice-based technological improvements [2].

Microdevices have been developed to characterize, monitor and detect many different types of analytes in different biological fluids. Microdevices and systems have been extensively studied for the analysis of proteins, cells and nucleic acids in clinical diagnosis and monitoring [2]. These efforts are usually categorized under the name of BioMEMS. Furthermore, the analysis of electrolytes such as sodium, potassium and

calcium and the concentration values of some analytes such as pH, urea, glucose in body fluids are important in biomedical applications. Electrochemical techniques have been one of the preferred methods to measure these parameters [2].

Electrochemical approaches, especially impedance measurements, have drawn great interest in the biomedical field due to rapid monitoring of minute changes at the electrode-solution interface [3]. Impedance measurement is an electrochemical approach and miniaturized impedance sensor designs and operations are indispensable part of the new technologies in both MEMS and BioMEMS fields.

Electrical impedance can be described as the ratio of applied voltage to the current passing through the device. The complex impedance of an electrode-solution interface can be characterized with its phase and magnitude values. They can also be represented as complex impedance values consisting of real and imaginary parts [1]. Unlike ideal electrical components, this impedance is non-linear and changes with both frequency and applied voltage bias [4]. Impedance measurements are made using a wide range of frequency and potential sweep, resulting in a spectrum of impedance. For the interpretation of impedance spectra, equivalent circuit models are needed [5]. Equivalent circuit model typically consists of resistance and capacitance values that model the physicochemical properties of the system [6].

The use of MEMS and BioMEMS in diagnostics and for POC mostly require labeling techniques, which use specific agents, probes, or redox reactions [2]. Such labeling techniques are time-consuming, complicated and need qualified labor work. Label-free electrochemical approaches can overcome these issues by giving fast, simple, low-cost, and miniaturized solutions. Non-faradaic electrochemical impedimetric sensors are in this category and can result in label-free detection. Impedance measurements can present alternative solutions to the challenges of labelling [1]. Impedance measurements can enable label-free operation by measuring the complex electrical resistance and capacitance values of electrochemical system [1] [6].

Label-free electrochemical impedance measurements depend on the surface po-

tential differences between samples and conductivity and capacitance which are the parameters to measure these changes [2]. By operating fast and label-free impedance measurements, the electrode surface changes of the analytes can be observed [3]. Recently, the development of lab-on-a-chip system for impedimetric sensors and biosensors has been the most attractive research area. Sensors are constructed to observe electrochemical changes at the surface of electrodes according to various analytes [5].

It is possible to evaluate the number of analytes in the solution as a function of the charge of impedance element related to resistance and capacitance values. The impedance measurement can be used to correlate the concentration of analytes at the selected frequency range. Most of the electrochemical studies use impedance results in Nyquist plot format, which plots real and imaginary part of the impedance [6].

Selvam et al. [6] designed a non-faradaic impedimetric high sensitive sensor. They used non-faradaic impedance to identify antigen-antiboy interactions by using cardiac biomarker named brain natriuretic peptide (BNP). Sensor has been fabricated on printed circuit board and interactions between antigen and antibody evaluated at low concentrations. The sensitivity results of sensor are determined by Nyquist plot analysis. Figure 1.1 shows the equivalent circuit of electrode solution interface and the peak value of Nyquist diagram shows low concentration of analytes.

Furthermore, impedance measurements have given rise to effective and simple measurements to obtain enormous information from droplets. In the field of microfluidics, droplet- based impedance sensors have advanced [7]. Droplet-based models are established to understand ionic charge accumulation (electrical double layer) near the surface of electrode [8]. Impedance is obtained at different frequencies and the obtained impedance spectra provides the characterization of the electrical double layer of the interface under the test [6].

Electrical double layer (EDL) plays an important role in the understanding of the interface between the charged surface and ionic solutions (e.g. body fluids). Electrical double layer is formed when excessive positive and negative ions in an aqueous solution

are ordered on solid surfaces [2] [9].

Electrical double layer has been studied in the literature for years regarding the understanding of surface structure and has been widely used in microfluidics, biomedical applications (e.g. drug carrier, cell, molecule and ion interactions), colloidal interactions, surface structure regulations [9]. Double layer and its capacitive behavior hinge on considerable parameters that include the material of electrode (metals, semiconductors etc.), solvent type, electrolyte, and temperature [10].

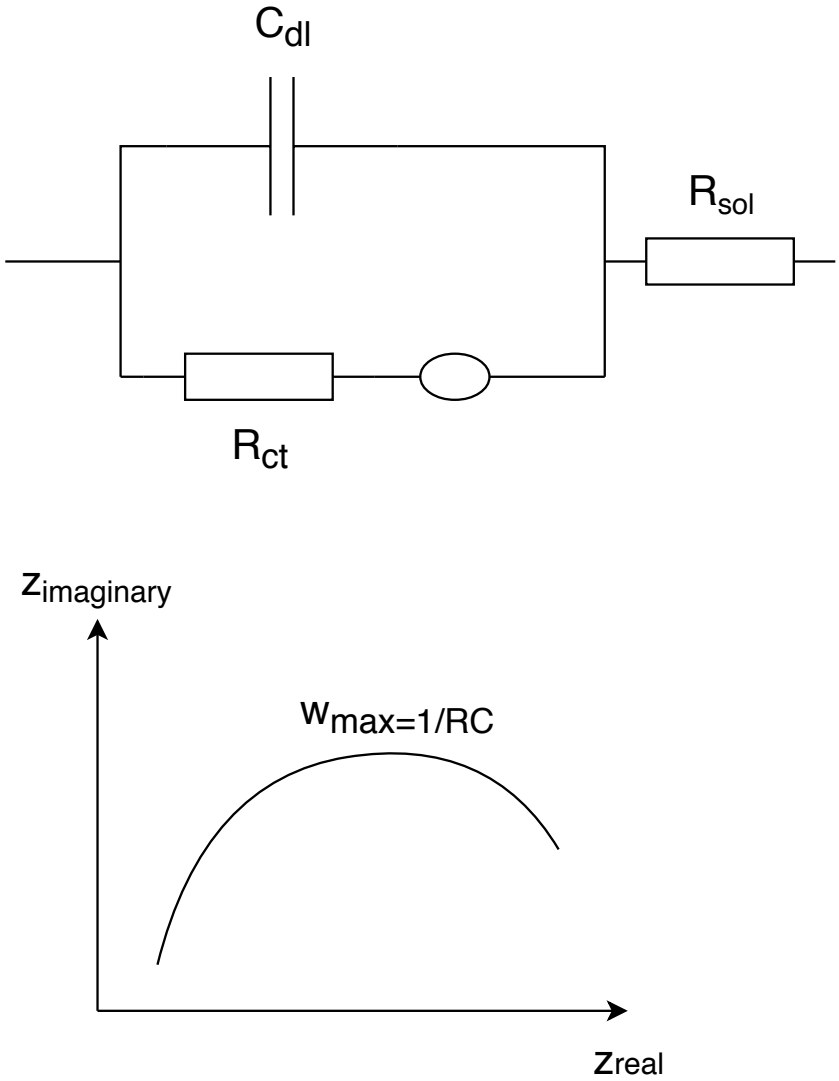

Figure 1.1 The equivalent circuit illustration for electrode solution interface from non-faradaic DNA detection and peak values show concentration of analytes [6].

The interfacial region is formed when an electrode is immersed in electrolyte

solutions [10]. Once a surface is plunged into an aqueous solution, a discontinuity occurs at the interface of the solution [11]. Charge separation occurs at the interfacial region due to the different chemical potentials between two phases. The thickness of EDL can change from 100 nm to couple angstroms. Electrical double layer can be 100 nm in a dilute solution and can reach a few angstroms in a more concentrated solution [11]. The double layer can be evaluated as a capacitor if the current flow on particular working electrode is measured by an electrical circuit [10]. When the double layer capacitor is charged properly to achieve desirable potential at working electrodes, capacitive current flows in the electrical circuit. By the time this capacitive current flows in the electrical circuit, it carries various information about both the double layer and its structure, and in many cases provides analytical results for electrochemical research [10]. The electrical properties of EDL are very important which they significantly influence electrochemical measurements [10]. EDL plays a significant role in electrochemistry. Many applications such as nanomaterial processing, sensor assembly can be mentioned related to electrical double layer [11].

Hence, understanding the EDL structure is the main consideration for the most of the research field. Multiple studies had been carried out to state and model non-faradaic processes and their sensing applications. Most of them stated mathematical models to EDL and related capacitances such as Helmholtz and Gouy-Chapman models [12].

The work in this thesis involves two steps to characterize the electrochemical non-faradaic impedimetric sensor. The first step is the measurement of different salt solution's (the range of concentration in between 0,001 M and 0,1M) impedance magnitude and phase angle values for different frequency and bias sweeps. Frequency sweeps are made from 20 Hz to 10 MHz at 0 V DC bias. Bias sweeps are mode from -1 V to +1 V DC at 20 Hz frequency. Double layer capacitance and solution conductivity values are extracted from the acquired data. These measurements characterize EDL according to ion size, concentration, and conductivity. Second step was to prepare pH solutions in a pH range between 2 to 11.50 at different concentrations (0.001 M to 0.1 M) and repeat the impedance measurement with the same parameters as before. This

way the effect of pH on EDL can be isolated using the previous salt solution EDL results.

In this study, gold (Au) interdigitated electrode was used to investigate the interface properties of analytes in terms of electrical double layer capacitance values in non faradaic region. Non-faradaic processes principle can be described as charge flow of current without charge transfer on the contrary to faradaic process that is based on the charge transfer onto the surface.

To eliminate the reaction on electrode-solution interface, reaction potentials of electrodes should be considered. We utilized Au electrode, hence, we conducted this study in -1 Volt to +1 Volt range. Because possible oxidation reactions at Au surface occur approximately 1 Volt [13]. Thus, chemical reactions were ignored on the Au electrode-solution interface.

According to the literature, most of the studies regarding impedimetric sensors have been made on Au electrode. Antibody immobilization on Au electrode to detect cancer cells and bacteria has been achieved by using monoclonal antibodies [3]. Impedimetric approaches for enzyme-based studies are based on the characterization only because of time-consuming frequency sweep for full impedance spectra [5]. One of the studies was conducted with gelatin-coated interdigitated Au electrode.They designed a biosensor to detect collagenase, which caused the change in impedance from interdigitated gold electrodes. Enzyme degradation of the layer produced a rapid rise in impedance when a critical thickness was reached. The change in impedance with protease digestion was correlated with solubilization of the gelatin layer from the sensor surface [14]. Furthermore, affinity based impedimetric sensors have gained attention. They can be performed by unskilled analysts and have potential to be used as multi-analyte sensors. For example, the study of an impedance immunosensor for human mammary tumor associated glycoprotein has been reported in literature that antibody was immobilized onto a gold electrode by spontaneous adsorption. Electrochemical characteristics were figured out by charge-transfer resistance obtained from Nyquist plot [5]. Additionally, several studies [15] were conducted on nucleic acid-based impedi-

metric sensors. By using a hanging mercury drop electrode, the differences between single-stranded (ss-DNA) and double helical conformations of nucleic acids and synthetic polynucleotides has been sensed. Electrical double layer of frequency dependence impedance and equivalent circuit model of the DNA-covered electrode were found in a complex impedance spectrum. Zhao et al. conducted a study on the impedimetric spectra of a bare gold electrode [5]. Unfortunately, none of these studies are label-free.

The inertness of gold (Au) electrode in electrochemical systems makes it an important choice for this study (the voltage of oxidation and reduction reactions of Au at gold electrode at the solution surface is illustrated at Figure 1.2. In this study, gold interdigitated electrode (AuIDE) was coated on glass wafer by a high vacuum thermal evaporator and patterned by lithography process and tested as a chemical sensor between the pH range of 2 and 11.50.

The fabricated AuIDE has 50 micrometer gaps between 200 micrometer wide interdigitated finger electrodes. The Au interdigitated electrodes were electrically characterized by impedance-frequency (Z-F) and impedance-bias voltage (Z-V) curves and Nyquist Plots.

In the second step of the study, pH measurement has been conducted on AuIDE electrode. Many chemical and biological processes such as blood monitoring, clinical tests and environmental monitoring [16]) are pH dependent and they track and record pH values [17]. pH sensors must be designed properly according to the accuracy and measurement range of the biomedical application. One of the applications that uses pH and impedance measurements togetheris pH-Impedance monitoring test which is commonly used for gastroesophageal reflux disease (GERD) diagnosis in clinics [18] [19]. GERD is a condition of the backflow of gastric contents (acidic, weakly acidic and weakly alkaline) towards esophagus [20] .Currently, separate impedance and pH probes are used for diagnosis. The measurement of impedance is based on the electrical impedance. Intraluminal thin probe which is closely arranged by electrodes is set to measure impedance of the stomach liquid. Electrode pairs reflects the impedance for each region of lumina. The probe is connected to voltage transducer that conveys the

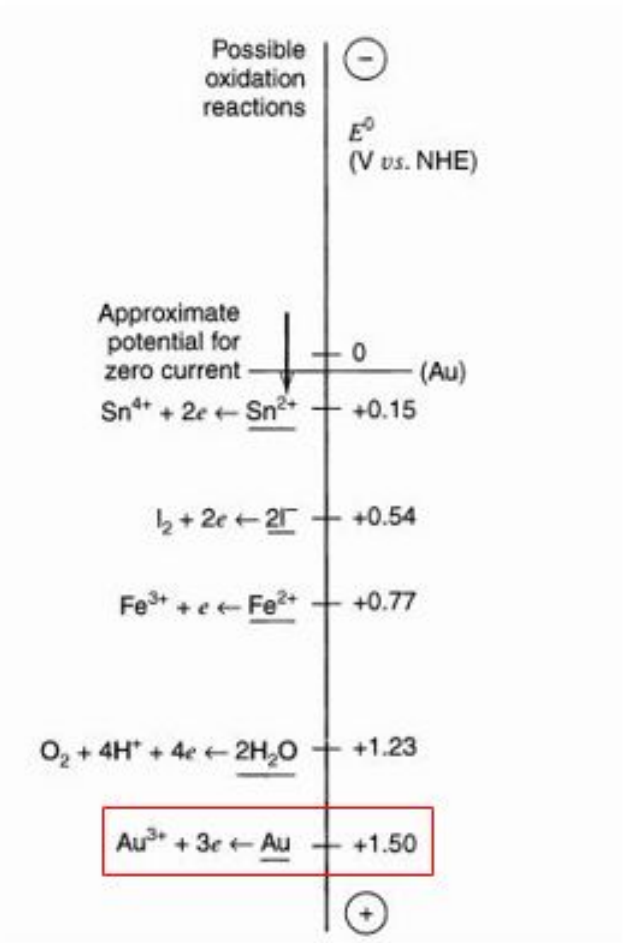

Figure 1.2 Illustration of oxidation and reduction reactions of gold electrode at the electrode-solution surface [13].

current. Impedance increases in the air (low conductivity) environment, and impedance decrease in the refluxed regions (high conductivity) [21]. The pH probe is used for the measurement of the acidic or alkaline condition of the disease. The characterization of non-faradaic impedimetric electrochemical sensor for different pH values in this work would enable usage of a single probe to do both impedance and pH measurements.

Conventional potentiometric tools to monitor pH variations are made up of large size ion selective electrodes which require more samples to monitor pH. However, it is crucial to be able to analyze pH changes of a micro-liter or less volume droplet samples, very quickly in medical field [22]. Biosensors and Lab-On-a-Chip technology try to achieve these kinds of pH sensors [23]. Interdigitated electrode-based pH detection has been studied in the literature very frequently. Rajapaska et al. used AuIDE on Silicon substrate fabricated by conventional photolithography method and electrically characterized according to current-voltage (I-V) measurements in the presence of various pH solutions (pH range between 3 to 12) to test the applicability of the electrode as a chemical pH sensor [23], and Azmi et al. also studied the aluminum interdigitated electrodes (IDE) on a silicon substrate that is fabricated by conventional photolithography method for pH sensing. The IDE was fabricated using standard photolithography process and they obtained electrical characteristics from current-voltage curves [24]. Another study also proposed that the aluminum IDE electrode for pH sensing applications and conducted small range of pH solutions (pH 4– pH 7 – pH 10) and electrical characteristics have been done by capacitance values of pH solutions [25]. However, according to these studies acidic and alkali solutions may not represent the precise pH levels in terms of I-V patterns because as shown at Figure 1.3, the I-V patterns of pH 4 and pH 10 are overlapping and it is hard to differentiate some of the pH levels.

In this study, we aim to explain both different salt and pH solutions according to their EDL values extracted from complex impedance value by impedance measurements. Each of the solution shows different EDL values. In electrochemistry, Nyquist plots have been used for good understanding of the interactions in electrochemistry and we also used this approach to evaluate our results.

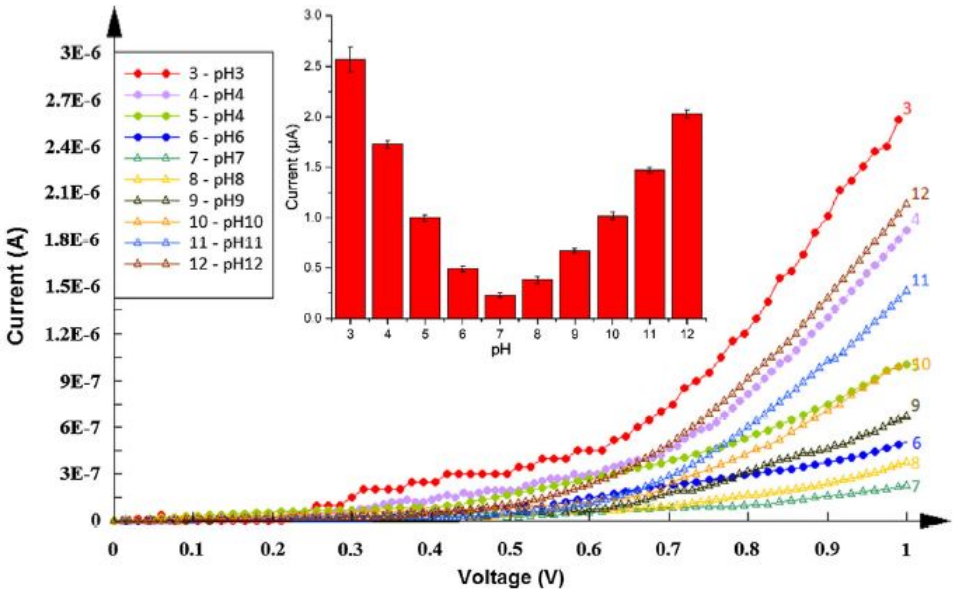

Figure 1.3 Measurement of acidic and alkali solutions. Test was conducted from pH 3 to pH 12 [23].

1.1 Motivation and Novelty

The diagnosis of many diseases stands in need for cost-effective and integrated diagnostic devices for detection and characterization of molecules in biomedical applications. The rapid technological developments in BioMEMS and nanotechnology offer new possibilities for improvement of sensor systems to achieve a set of analysis with cost-effective, on-demand, rapid, high throughput point of care diagnostics.

The recent advances in microfluidics have paved the way for the achievements of analyte handling from millions of droplets with high performance, label free electrical measurements for biological applications such as molecule detection, drug screening, and biological assays in body fluids. If the improvements associated with electrical droplet based sensors are addressed properly, their contribution will significantly widen the application space of the LoC developments for exceptionally delicate, on-demand, minimal effort screening. Impedance measurements have given rise to effective and simple measurements to obtain enormous information from droplets. For a wider scope of applications, in any case, all droplet based models should be established to contain

ionic charge accumulation (electrical double layer) near the surface of the electrode.

In this regard, this study investigated a theoretical model of non-faradaic impedance of a micro-sized droplet and developed the model by measurements comprising different analyte concentrations accumulated on the electrode surface.Impedimetric sensors require no extra reagents and provide real-time, label free analyzing and non-destructive and non invasive tool for POC medical applications. This study is designed, for the first time, to characterize non-faradaic label-free electrochemical impedimetric sensor regarding a broader range of analyte concentrations including three different salt solutions and various pH solutions by obtaining the EDL capacitance and Nyquist plots.

1.2 Outline of the Thesis

The brief summary of point of care technologies and MEMS and their relationship between biological and clinical environment and the main purpose of the thesis are stated at the introduction section. In section 2, fundamental theories and models related to impedance and electrical double layer are mentioned. Paper continuous with the experimental procedures and results at section 3 and 4. The final part of the thesis is the conclusion part where results are evaluated and future work is mentioned is at the section 5.

2. FUNDAMENTAL THEORIES

2.1 Electrochemical Principles

Electrochemistry is part of a chemistry science and referred to the interrelation between electrical and chemical events. This branch mostly considers the research of chemical changes due to an electrical energy and electric current caused by chemical reactions [13]. Electrochemical approaches can be used for several reasons such as electroanalytical sensors [13], detection of proteins and molecules [26], purification studies [27], surface analysis [28] [29]. In general, electrochemistry is a process which takes place at electrode-solution interface and determined by the properties of both electrode and solution [30]. In most of the studies, electrochemical approach is used to analyze a solution for determination of metal ions and organic groups. Electrochemical methods, hence, require a deep understanding of a basic principles of the electrode-solution interfaces [13].

Electrochemical cells are defined as the separation of two electrodes by an electrolyte or electrolytes. In the systems of electrochemistry, processes cause the charge transfer between chemical phases, for instance, an electrode and an electrolyte. Electrode materials mostly include solid metals (Au, Pt, etc.), carbon, liquid metals, and semiconductors (e.g. Si). Charge is carried in the electrolyte by the motion of ions. Liquid electrolyte solutions carrying ions, like H+, Na+, Cl- can be in water or non-aqueous solvents. To provide effectiveness of electrochemical cell, the electrolyte-solvent structure should be sufficiently conductive [13].

2.2 Explanation of Non-Faradaic Processes

In a simple electrochemical cell, two electrodes are immersed in an electrolyte solution. A voltage potential is developed between electrodes when an electrical power

supply is connected. If the applied voltage value exceeds the cell potential of the electrochemical cell, this potential produces current flow at the outside of the circuit owing to the charge transfer which induces oxidation and reduction reactions. These reactions are explained by Faraday's Law as the proportionality of the quantity of charges passing through the cell to the amount of chemical reactions happening and in at Figure 2.1 shows the simple representation of oxidation and reduction reaction at electrode-electrolyte surface. [13].

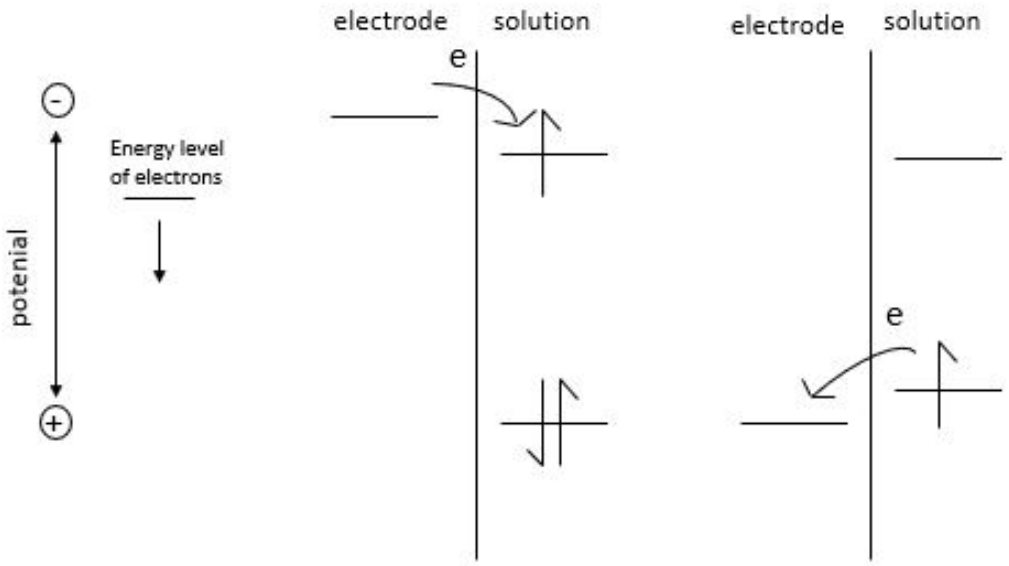

Figure 2.1 Illustration of oxidation and reduction reactions at the electrode-solution surface [13].

However, in some processes (e.g. thermodynamically and kinetically improper conditions) charge transfer (chemical reactions) cannot occur along the electrode- electrolyte interface and the interface can show a potential range. These processes are called non-faradaic processes. Adsorption and desorption can still be seen at the electrode-electrolyte interface. Furthermore, this interface can be altered with solution composition or changing potential. If solution composition, applied potential or electrode surface area are altered, outside currents could flow through the cell even though charge does not pass through the interface, meaning that no electrochemical reaction is taking place [13]. Non-faradaic processes primarily focus on charge transfer and related reactions to obtain information from electrochemical data [13].

2.3 Electrical Double Layer

If a potential is applied across the two metal electrodes immersed in an electrolyte, and assuming no electrochemical reaction takes place, the behavior of metal-solution interface behaves like a capacitor which is an electrical circuit element formed by two metal sheets separated by a dielectric material. This behavior can be shown by an equation below [13]:

$$C = \frac{q}{E} \tag{2.1}$$

where q is the stored charge on capacitor in Couloumbs (C) and E is the potential crossing capacitor in Volts (V), and C is the capacitor in Farads (F).

Charge accumulates on the metal surface till q satisfies the equation. Along the charging, charging current flows and there are excessive electrons on one metal plate and deficit electrons on the other plate. There is no charge transfer observed across the metal-solution interface. Such an electrode is called ideal polarizable electrode (IPE) as shown in at Figure 2.2.

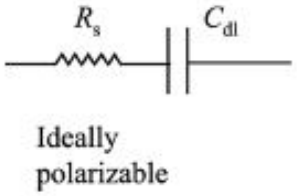

Figure 2.2 Equivalent circuit model for ideally polarizable interfaces where R_s is the solution resistance and C_{dl} double layer capacitance [11].

The current magnitude, on the other hand, depends on the circuit resistance. At an applied potential, there will be a charge both on the metal electrode (q^m) and in the solution (q^s). There can be a negative or positive charge on the metal surface depending on the given potential and the solution composition (Figure 2.3 and Figure

2.4, shows the capacitor and the charged capacitor respectively). The excessive and deficit charge on the metal electrode (q^m) is located in very thin layer. The excess of either cations or anions in the solution reside around the surface of the electrode. These excessive charges are usually separated by the electrode area called charge densities ($\sigma^m = q^m/A$) often shown as $\mu C/cm^2$. the overall array of charged species and dipoles at the electrode surface called electrical double layer and the electrode-solution interface is characterized by a double layer capacitance, C_d, (μF) at a given potential and EDL is usually a function of potential [13].

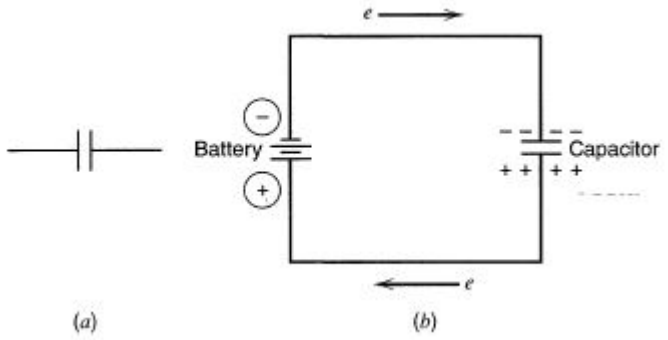

Figure 2.3 (a) a capacitor and (b) charged capacitor [13].

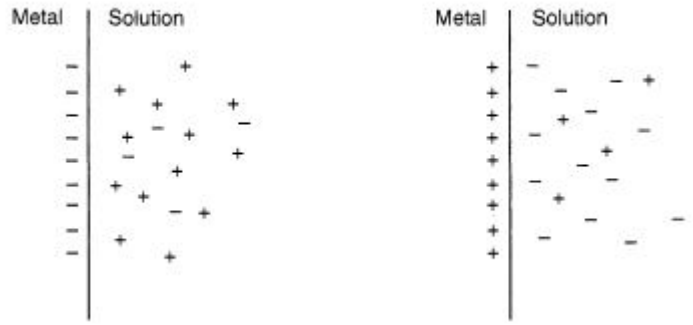

Figure 2.4 Negatively and positively charged metal-solution interface [13].

The double layer is assumed to be composed of multiple layers. The layer closest to the electrode at the solution side has several names like inner, compact, Helmholtz and also Stern layer. This layer is composed of solvent molecules and sometimes ions and molecules that are specifically absorbed [13]. The location of the electrical center of these specifically absorbed dehydrated ions is named as inner Helmholtz plane (IHP) and the electrical center of the nearest hydrated counter ions is named as outer Helmholtz plane (OHP) [11] which are represented at Figure 2.5 and Figure 2.7. The ions outside of the OHP are distributed into the bulk of the solution and in balance with the charged metal surface by electrostatic forces and thermal diffusion. This region is called diffuse layer or Gouy–Chapman layer [11] [13].

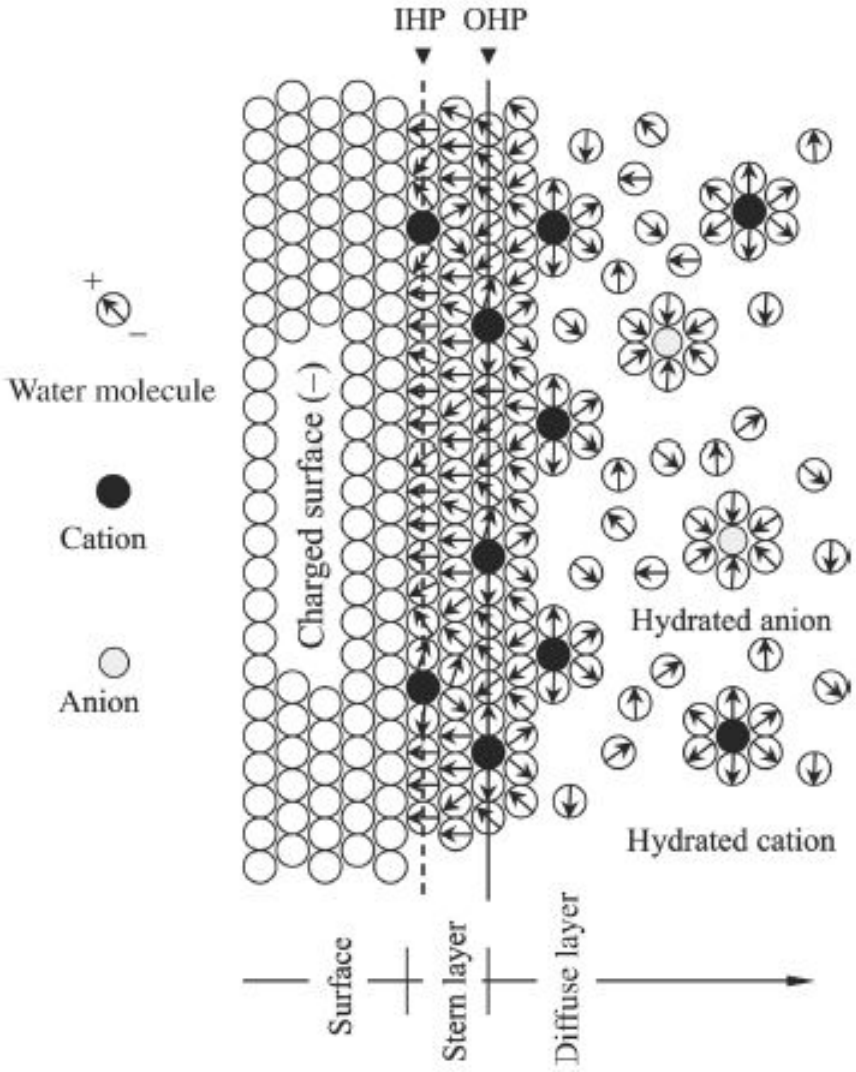

Figure 2.5 The illustrative model of EDL at ideally polarizable interface [11].

2.3.1 Theoretical Models for Double Layer Structure

2.3.1.1 The Helmholtz Model. The idea of the electrical double layer was first thought by Helmholtz [31]. This is the idea of charge separation at the interface. He proposed that charged surface in electrolyte solution repels the same charge ions but attracts counter-charge ions and there would be two layer which is formed by charge at the electrode surface and counter-charge ions in the electrolyte that has been called electrical double layer [32] as represented at Figure 2.6.

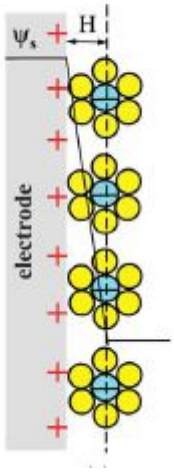

Figure 2.6 Electrical double layer representation according to Helmholtz model and H is the approximated radius of ions to conventional planar electrodes and ψ is the potential at the electrode surface [32].

Since the structure is analogous to parallel plate capacitor, the relation of charge density (σ), voltage (V), the dielectric constant (ε), permittivity (ε_0), and inter-plate space (d) can be explained by the equation below:

$$\sigma = \frac{\varepsilon\varepsilon_0}{d}V \tag{2.2}$$

Hence, the differential capacitance is given as [13]:

$$\frac{\partial \sigma}{\partial V} = C_d = \frac{\varepsilon \varepsilon_0}{d} \tag{2.3}$$

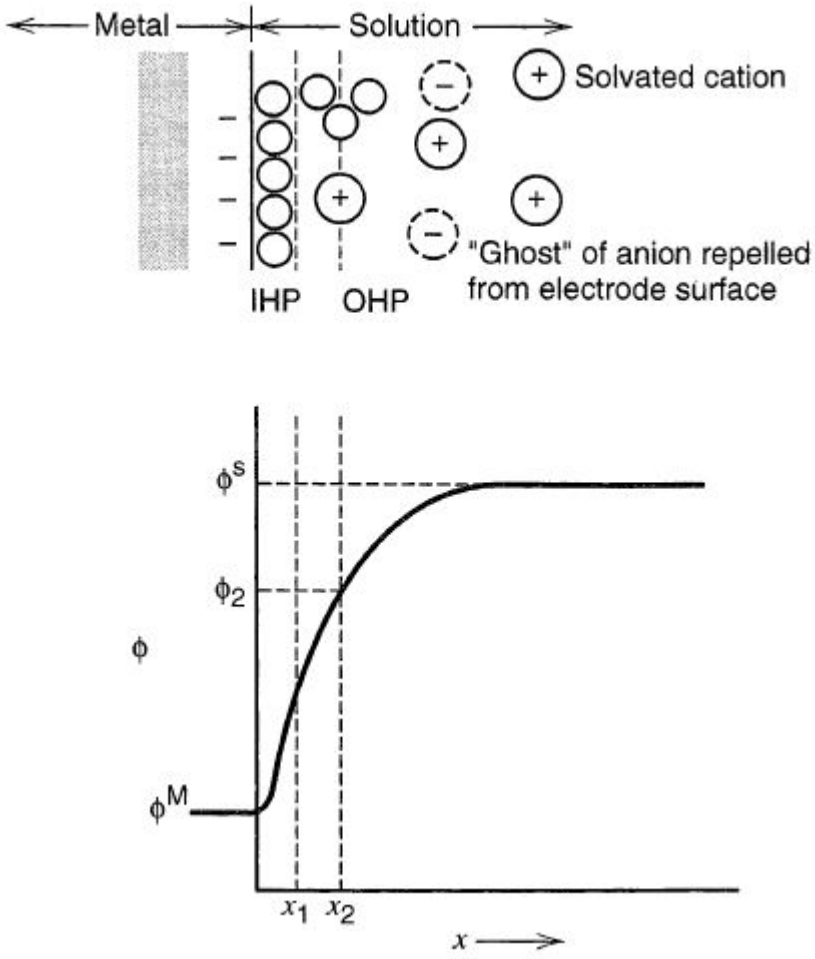

Figure 2.7 Potential profile along the double layer regardless of specific ion adsorption where ψ represents the inner potential [13].

2.3.1.2 The Gouy-Chapman Model. According to the Helmholtz model, the differential capacitance should be constant, but the charge is confined to the electrode surface, the same concept is not generally valid for the solution (at Figure 2.8) [13]. Gouy-Chapman model independently proposed the concept of diffuse layer which depends on the Boltzmann equation [13] and suggest that the ion distribution should be continuous in the solution. The compression of diffuse layer should occur with the increase of electrolyte concentration, and consequently this should be seen as a rise in

capacitance [32]. The assumed differential capacitance according to Gouy-Chapman theory is illustrated as at Figure 2.9 in the literature. Figure 2.10 shows the experimental results of NaF concentration and differential capacitance relationships at the mercury surface [13].

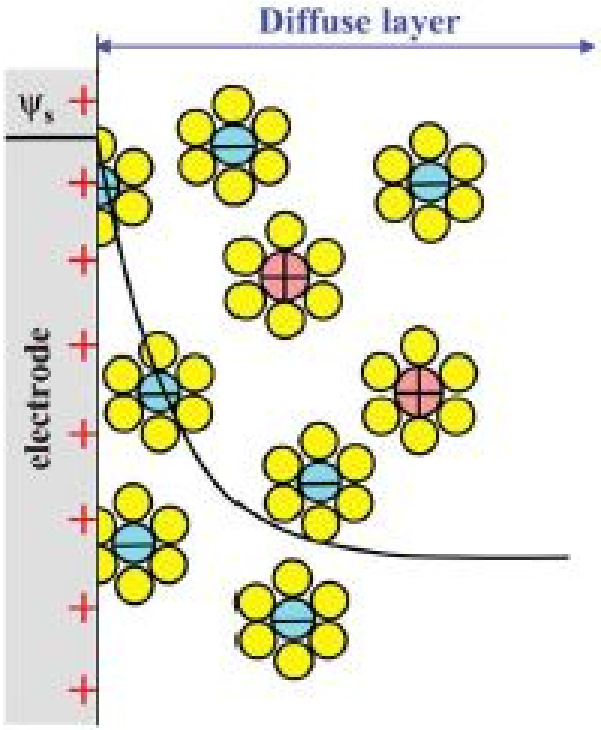

Figure 2.8 Electrical double layer representation according to Gouy-Chapman model and H is the approximated radius of ions to conventional planar electrodes and ψ_s is the potential at the electrode surface [32].

Therefore, the differential capacitance of the diffuse double layer, Cd, can be expressed as [13]:

$$C_d = \sqrt{\frac{2z^2q^2\varepsilon\varepsilon_0 n^0}{kT}}\cosh(\frac{zq\psi_0}{2kT}) \tag{2.4}$$

The simplified equation 2.4 for dilute aqueous solutions can be given as at 25 °C and |z| = 1 and C_d is $(\mu F)/cm^2$ with,

z= the (signed) charge of ion,

q= the charge unit,

ε= the solution permittivity,

ε_0= the air permittivity ,

n_0= the number of ions in the solution,

k= the Boltzmann's constant,

T= the temperature

ψ_0= the electrostatic potential at the surface regarding bulk solution.

$$C_d = 228\sqrt{I_0}\cosh(19.5\psi^0) \tag{2.5}$$

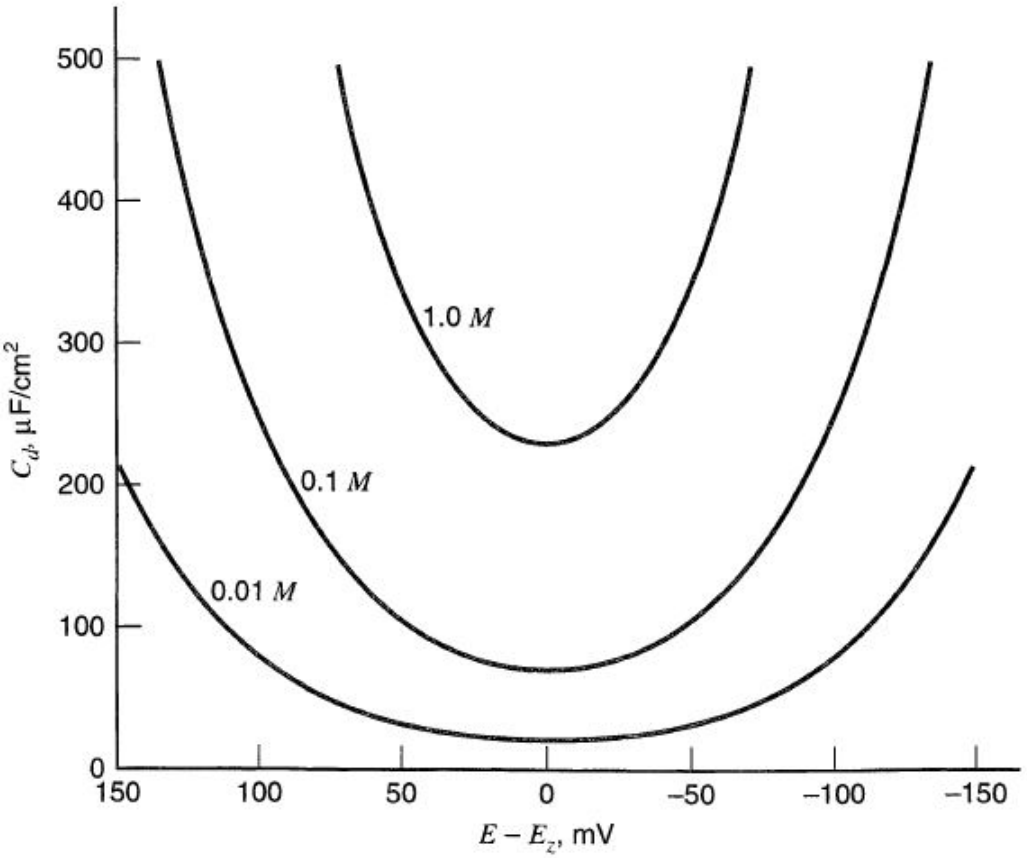

Figure 2.9 Assumed differential capacitance according to theory of the Gouy-Chapman at 25 °C [13].

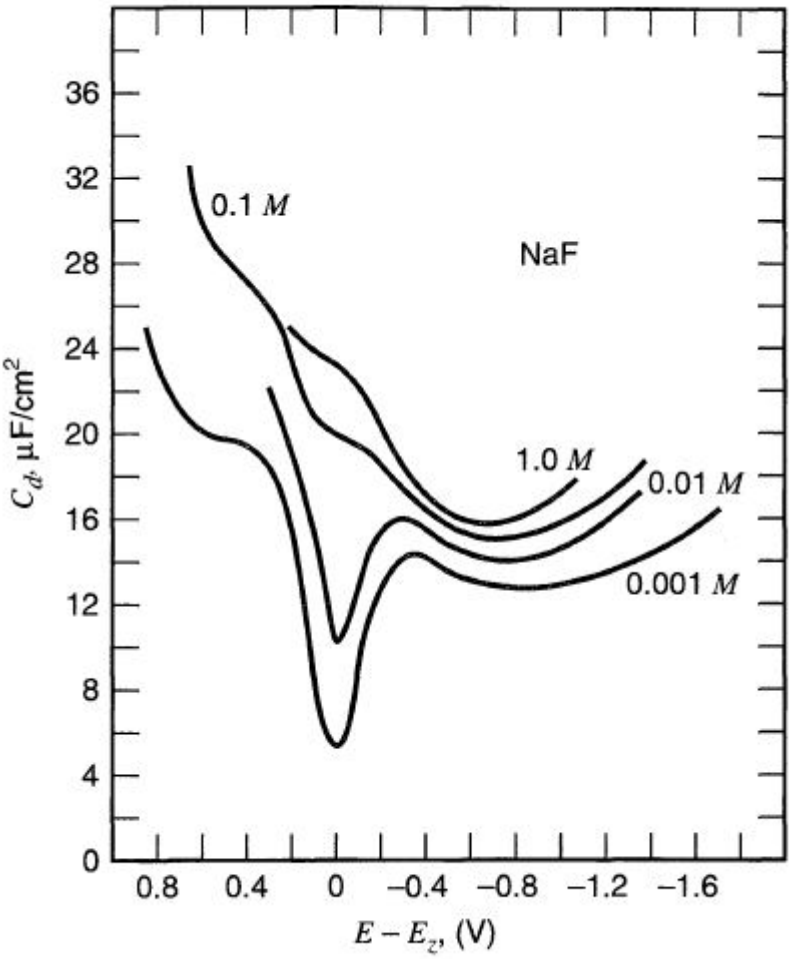

Figure 2.10 The differential capacitance of NaF solution at the mercury surface at 25°C with respect to potential changes [13].

2.3.1.3 The Modification of Stern. Because of the limitless rise in differential capacitance with potential in Gouy-Chapman model [13], a new model was proposed by Stern in 1924 [32].

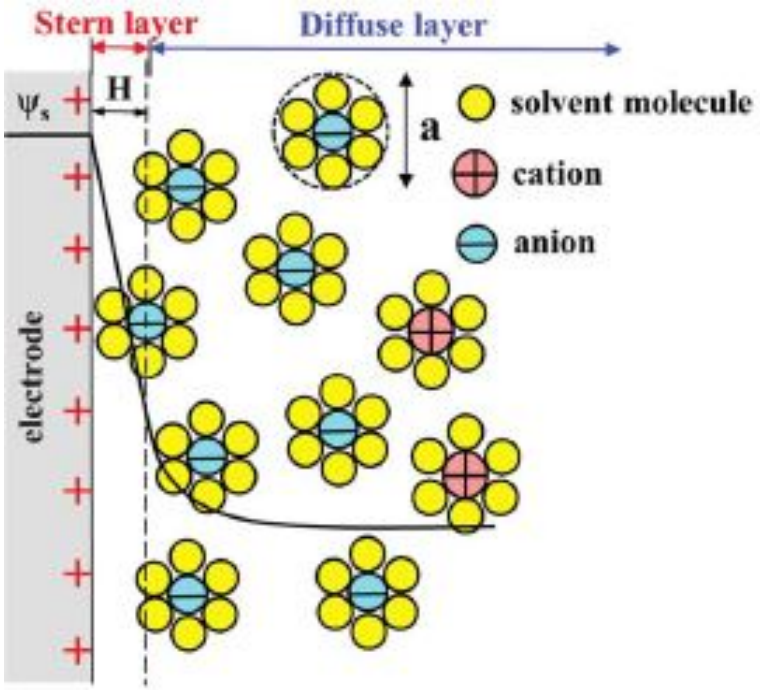

Figure 2.11 Electrical double layer representation according to Gouy-Chapman-Stern model and H is the approximated radius of ions to conventional planar electrodes and ψ_s is the potential at the electrode surface [32].

Electrical double layer operates as a capacitance and the charge density at the surface rises if the potential at the surface is increased [11]. Since Stern and diffuse layer are distinct from each other as shown at Figure 2.11, it is rational to separate them into series of two components reciprocally as shown in equation below where C_H is the the Stern-layer and C_D is the diffuse-layer capacitance at Figure 2.12. C_d exhibits a complex characteristics and determined by the smaller one of C_D and C_H [13].

$$\frac{1}{C_d} = \frac{1}{C_H} + \frac{1}{C_D} \tag{2.6}$$

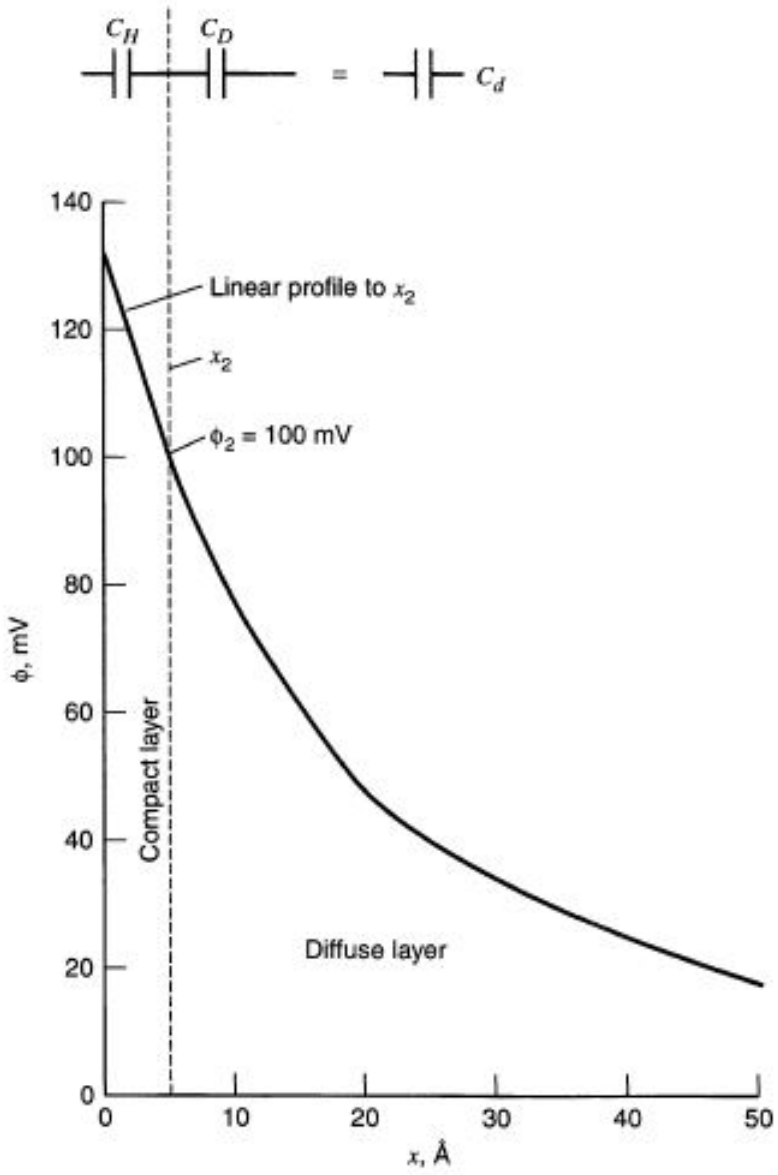

Figure 2.12 A series model of differential capacitance and a illustrative profile of EDL from the solution side according to Gouy-Chapman-Stern model [13].

It is expected to be seen V-shaped pattern of C_D at low concentration of electrolyte in the systems of potential zero charge (PZC), and at high electrolyte concentrations or high polarized dilute media C_D gets larger and do not affect the C_d and only stable capacitance of C_H can be seen [13]. This assumption is illustrated as at Figure 2.13 in the literature.

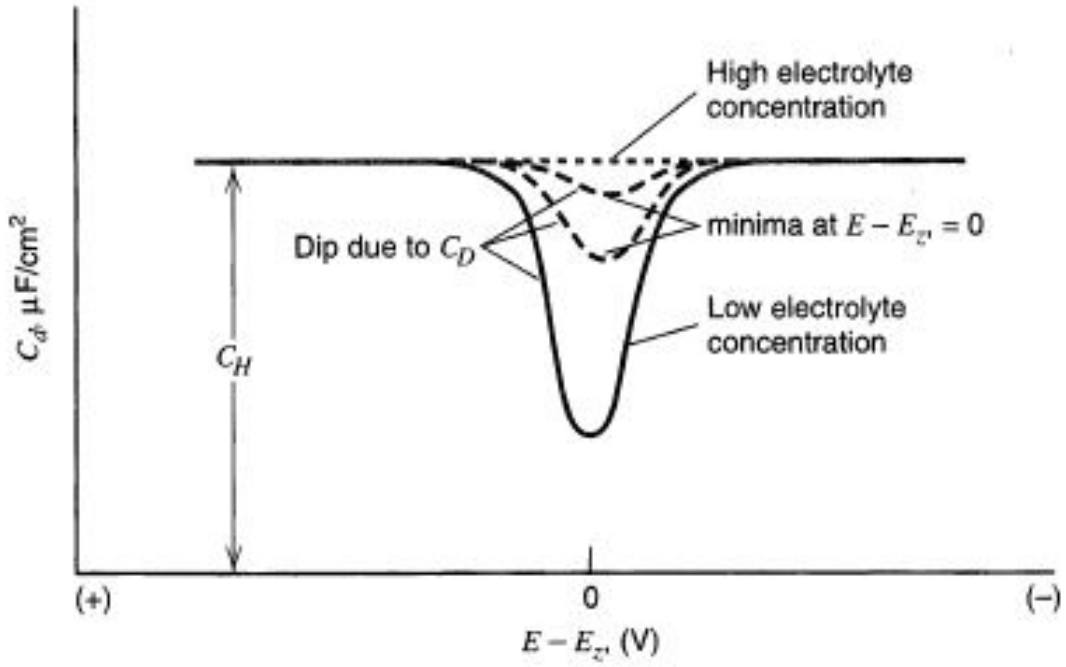

Figure 2.13 Assumed characteristics of C_d as stated in Gouy-Chapman-Stern model [13].

2.3.2 Impedance

Impedance (Z) can be described as the total amount of opposition to the flow of direct or alternating current passing through the circuit at given frequency in electrical devices and the unit of impedance is Ohm (Ω). Impedance is expressed as complex (two dimensional) number and includes real and imaginary parts and shown in vector plane. Real part and imaginary parts represent resistance (R) and reactance (X) respectively. The expression of impedance is shown at the rectangular coordinate in Figure 2.14. The polar form of the impedance is represented as magnitude |Z| and phase angle θ [33].

The mathematical expression of impedance;

$$Z = R + jX \tag{2.7}$$

$$R = |Z|cos\theta \tag{2.8}$$

$$X = |Z|sin\theta \tag{2.9}$$

$$|Z| = \sqrt{R^2 + X^2} \tag{2.10}$$

$$\theta = tan^{-1}\frac{X}{R} \tag{2.11}$$

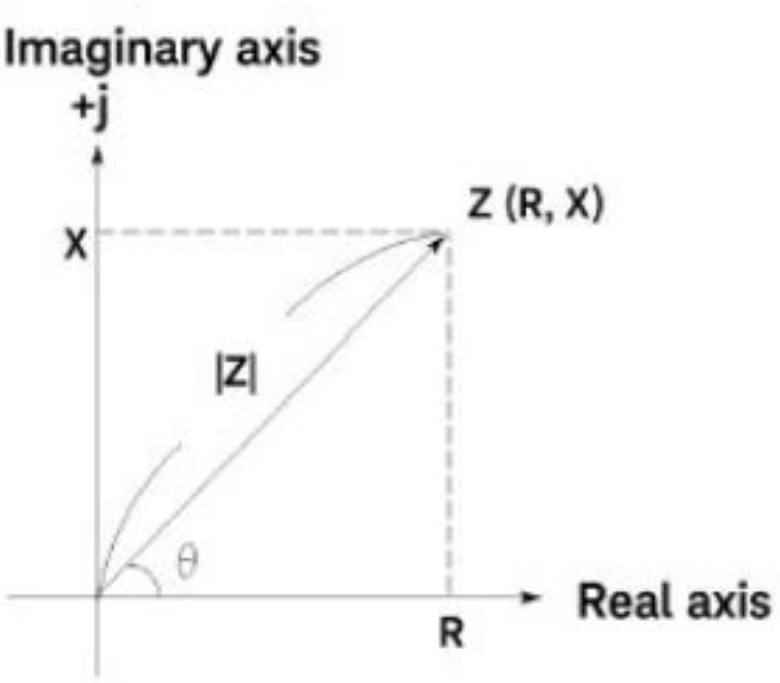

Figure 2.14 Impedance at rectangular coordinate [33].

3. METHODOLOGY

3.1 Experimental Setup

3.1.1 Impedance Measurement

Impedance measurements were conducted on the Impedance Analyzer (Keysight Technologies E4990A) which can be seen in at Figure 3.1. It can measure both the exact impedance magnitude value and the phase angle by either sweeping the frequency between 20 Hz and 10 MHz or the DC bias from -20 V to +20 V.

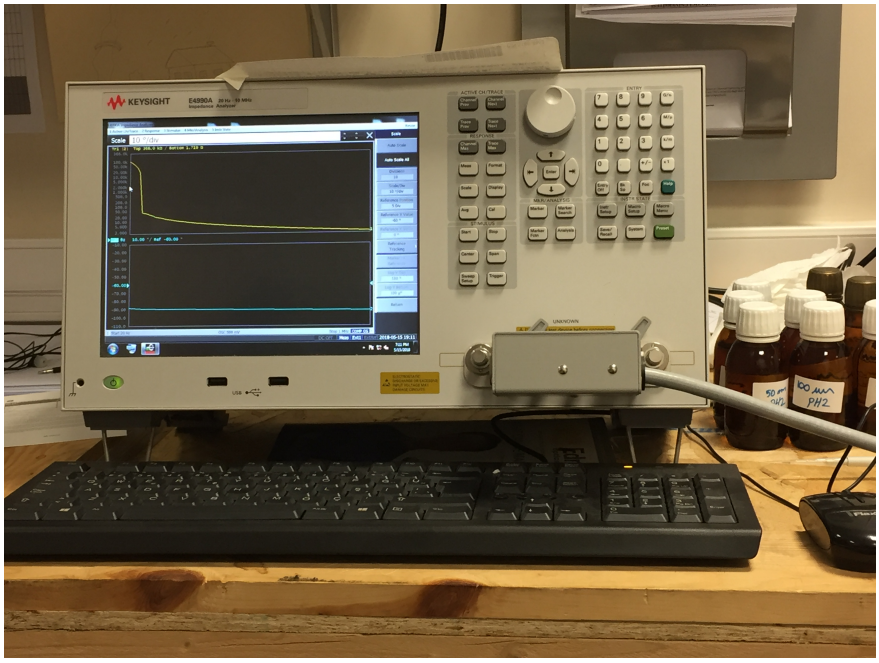

Figure 3.1 Impedance Analyzer.

.

Figure 3.2 Impedance Analyzer and shielded electrode measurement box.

Impedance measurements were carried for both Z-F and Z-V curves. Z-F measurements were taken at a frequency range between 20 Hz to 10 MHz with an AC signal amplitude of 10 mV at 0.0 V DC Bias and Z-V measurements were taken at a voltage range from -1.0 V to +1.0 V with an AC signal amplitude of 10 mV and at 20 Hz constant frequency.

Before each measurements, the equipment was calibrated for open and short circuit and known load circuit.

The device under test was shielded using a grounded metal case to prevent from noise from surrounding environment as shown in at Figure 3.2.

3.1.2 Solution Preparation

- **Salt Solutions;** Lithium Chloride (LiCl), Sodium Chloride (NaCl) and Potassium Chloride (KCl) salts were used to prepare different molarity salt solutions. They were dissolved in 100 mL of de-ionized water. Table 3.2 gives the specific weights used in the preparation of each salt solution.

Table 3.1
Molecular weights of LiCl, NaCl and KCl.

LiCl (g/mol)	NaCl (g/mol)	KCl (g/mol)
42.39 g/mol	58.44 g/mol	74.55 g/mol

Table 3.2
Weights used in preparation of salt solutions.

Solution Molarity (M)	LiCl (g)	NaCl (g)	KCl (g)
0.001 M	0.004239 g	0.005844 g	0.007455 g
0.002 M	0.008478 g	0.0116 g	0.01491 g
0.005 M	0.021195 g	0.029 g	0.037 g
0.01 M	0.04239 g	0.05844 g	0.07455 g
0.025 M	0.1059 g	0.145 g	0.01863 g
0.05 M	0.21195 g	0.290 g	0.3727 g
0.1 M	0.04239 g	0.5844 g	0.7455 g

- **pH Solutions;**

  pH 2.00, pH 3.00, pH 4.00, pH 5.00, pH 6.00, pH 7.00, pH 8.00, pH 9.00 and pH 11.50 solutions were prepared in 1 mM, 10 mM, 50 mM and 100 mM concentrations.

  To prepare pH solutions, strong acid (Hydrochloric Acid) and strong base (Sodium Hydroxide) were used. Both NaOH and HCl ionize completely in aqueous solutions.

Ionization of NaOH an HCl in aqueous solution;

$$HCl_{(aq)} + H_2O_{(l)} \rightarrow H_3O^+_{(aq)} + Cl^-_{(aq)} \tag{3.1}$$

$$NaOH_{(s)} \rightarrow Na^+_{(aq)} + OH^-_{(aq)} \tag{3.2}$$

To calculate the pH, equations 3.3,3.4,3.5 were applied.

$$pH = -log_{10}[H^+] \tag{3.3}$$

$$pOH = -log_{10}[OH^-] \tag{3.4}$$

$$pH = pH + pOH \tag{3.5}$$

Firstly, pH 11.50 stock solution was acquired and diluted to prepare pH 4, pH 5, pH 6, pH 7, pH 8, pH 9 solutions using the equation below;

$$M_1V_1 = M_2V_2 \tag{3.6}$$

For the preparation of basic solution, NaOH was used which has 40 g/mol molecular weight. We prepared $10^{-2.5}$ M NaOH solution (126.4 mg NaOH added to 1 liter DIW) and obtained $10^{-2.5}$ M OH^- ions since NaOH is a strong base and ionizes completely and produce the same molarity of OH^- ions in the solution. We took the negative log of $10^{-2.5}$ found the pOH as pH 11.50.

The equation 3.6 gives rise to form other pH solutions from pH 11.50 stock solutions.

Table 3.3
Weighted Sodium Chloride to prepare 1 mM, 10 mM, 50 mM and 100 mM concentrations.

Molarity (M)	NaCl (g)
1 mM	0.005844 g
10 mM	0.05844 g
50 mM	0.290 g
100 mM	0.5844 g

Secondly, pH 2.00 and pH 3.00 acidic solutions were prepared by using HCl. Chemical properties of fuming 37% HCl;

37% w/w $HCl_{(aq)}$ has a density of 1.19 kg/L.

Molecular weight of HCl = 36.5 g/mol.

Molar conversion;

% w/w HCl to w/v HCl: 37% HCl x 1.19 kg/L density = 0.44 kg/L HCl w/v to mol/v: 0.44 kg/L / 36.5 g/mol = 12 mol/L

Therefore, concentrated HCl 37% is 12 molar (= M = mol/L).

Diluted HCl from concentrated HCl;

1M HCl: add 1mol/12M = 83 ml conc. HCl to 1L of water or 8.3ml to 100ml.

pH 2.00 and pH 3.00 solutions were prepared by dilution of HCl to 0.01 M and 0.001 M and NaCl weighted (Table 3.3 shows the weighted amounts of NaCl (g)) and dissolved in 100 ml pH 2.00 and pH 3.00 solutions.

3.2 Fabrication of Gold Interdigitated Electrode

Cr-Au coated glass wafer was used to make micro-electrodes. Cr and Au were deposited on the glass wafer (SiO_2) using high vacuum thermal evaporator. Lithography process and wet etching were applied to pattern thin film of Cr/Au layer as micro-electrodes. The thin film of metal was coated with photoresist and IDE mask

put on the sample. After 2 minutes UV light exposure IDE pattern was transferred to the photoresist. In the photoresist (Pr) development process, Pr developer was utilized to remove Pr in the exposed region. Subsequently, the sample was undergone to Au and Cr etchant for 2-3 minutes to remove the exposed area. Lastly, acetone was used to remove photoresist. Cr-Au electrode has 16 fingers with 50 μm gaps 200 μm widths.

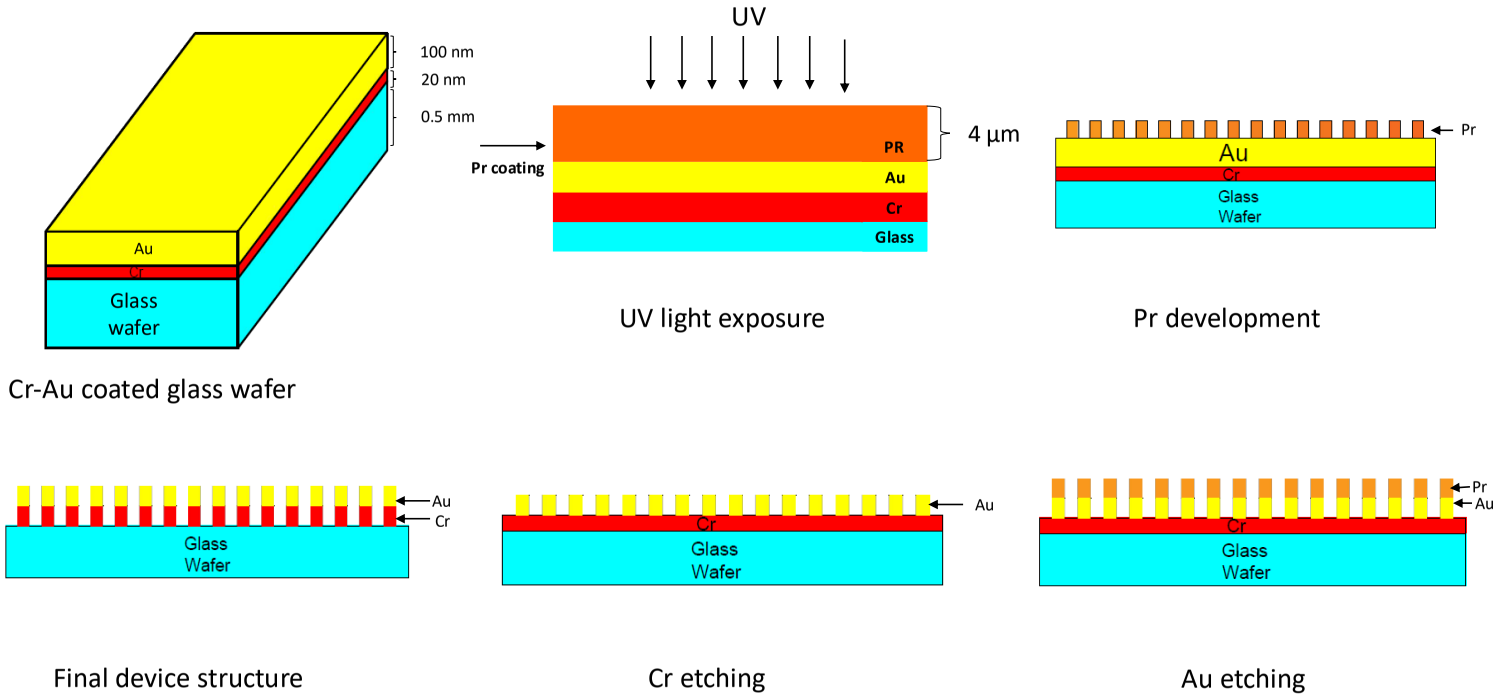

Figure 3.3 The consecutive steps of AuIDE fabrication.

.

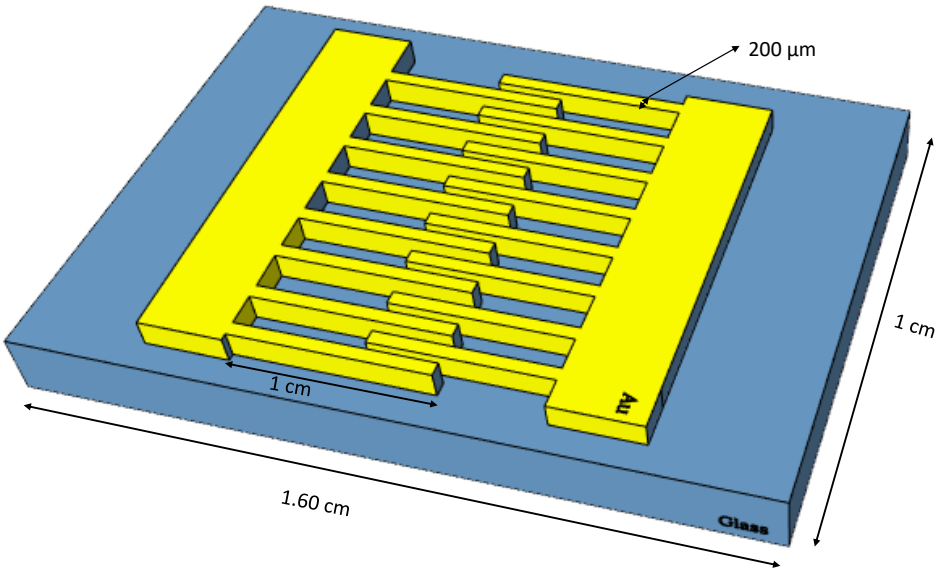

Figure 3.4 Dimensions of AuIDE electrode.

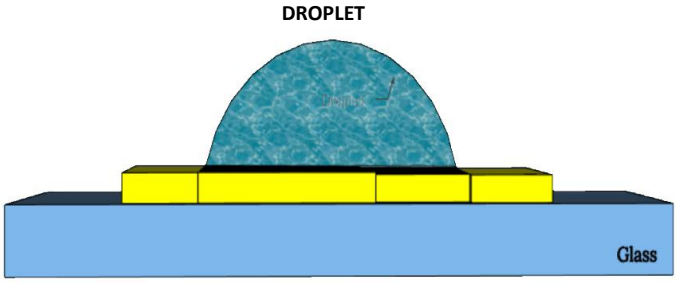

Figure 3.5 Illustration of droplet on the AuIDE.

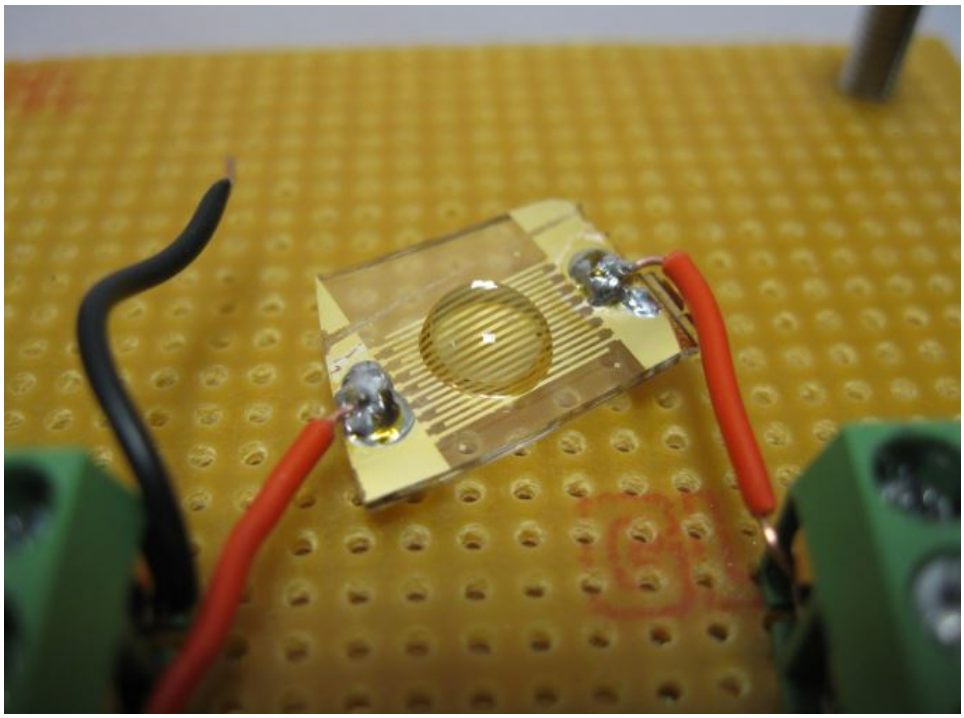

Figure 3.6 Device under test: Solution droplet on the AuIDE.

.

3.3 Mathematical Modelling of Impedance Data

Impedance is a complex phenomenon consisting of chemical, electrical, physical and mechanical components. Equivalent circuit model is a must to fit impedance data according to the electrochemical processes in the systems under investigation.

Resistors and capacitors are mostly applied as ideal circuit elements. However, to define the nonlinear impedance of real systems, distributed circuit systems such as CPE (Constant Phase Element) are required in addition to the ideal circuit elements. Double layer capacitor generally does not behave ideally because of the current distribution and also electroactive species in the systems. Rather double layer capacitance behaves like a CPE which is mostly used in impedance data modeling [34].

$$CPE = \frac{1}{C_{dl}(jW)^{\alpha}} = \frac{1}{C_{dl}W^{\alpha}}(\cos(\frac{\prod \alpha}{2}) - j\sin(\frac{\prod \alpha}{2})) \tag{3.7}$$

C_{dl} is the CPE coefficient ($(ohm^{-1}.s^{\alpha})$. For condition that C_{dl} is equal to C (pure capacitor) and, the exponent, α is equal to 1 give the impedance of pure capacitor and if α is equal to 0 the equation results in $C_{dl} = \frac{1}{R}$ which is an impedance response of an ideal capacitor [34].

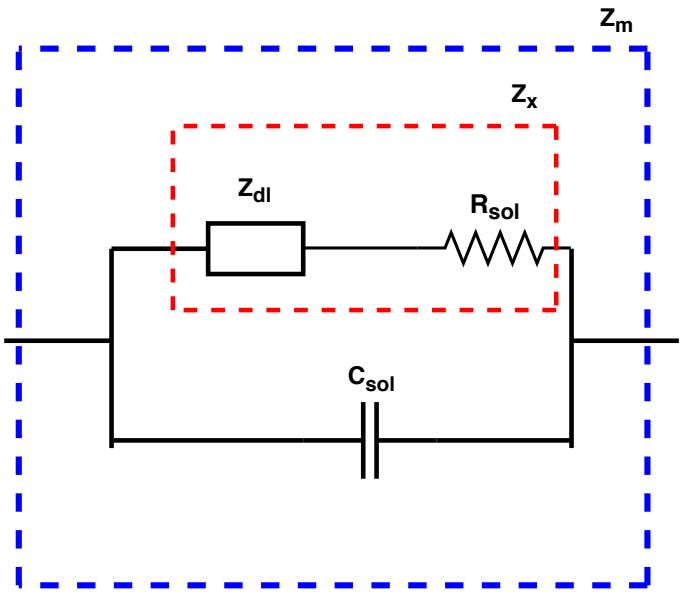

Figure 3.7 Equivalent circuit model.

.

Non-faradaic response of a two-electrode electrochemical cell can be modelled as shown at Figure 3.7, In this model, R_{bulk} (will be named as R_{sol}) models the linear electrical resistivity between two electrodes. C_{bulk} (will be named as C_{sol}) models the capacitance formed between two electrodes due to the dielectric nature of the solution. According to this model, R_{bulk} and C_{bulk} values dominate the impedance value at the high frequencies because at the high frequencies double layer impedance is becoming

short-circuited. The given model simplifies to parallel combination of $R_{bulk}|C_{bulk}$ at high frequencies.

First step of the data extraction is to find solution resistivity and capacitance (R_{sol}, C_{sol}) at high frequencies:

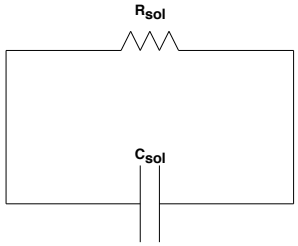

Figure 3.8 $R_{sol}|C_{sol}$

.

$$Z_{(C_{sol})} = \frac{-j}{W.C_{sol}} \tag{3.8}$$

$$Z_{(R_{sol})} = R_{sol} \tag{3.9}$$

$$Z_{sol} = \frac{R_{sol}(\frac{-j}{WC_{sol}})}{R_{sol} + \frac{-j}{WC_{sol}}} \tag{3.10}$$

$$Z_{sol} = \frac{-R_{sol}j}{R_{sol}WC_{sol} - j} = \frac{-R_{sol}j(R_{sol}WC_{sol} + j)}{R_{sol}^2W^2C_{sol}^2 + 1} \tag{3.11}$$

$$Z_{sol} = \frac{R_{sol}}{R_{sol}^2 W^2 C_{sol}^2 + 1} - \frac{j R_{sol}^2 W C_{sol}}{1 + R_{sol}^2 W^2 C_{sol}^2} \tag{3.12}$$

Real part of Z_{sol} ;

$$\frac{R_{sol}}{R_{sol}^2 W^2 C_{sol}^2 + 1} \tag{3.13}$$

Imaginary part of Z_{sol} ;

$$\frac{j R_{sol}^2 W C_{sol}}{1 + R_{sol}^2 W^2 C_{sol}^2} \tag{3.14}$$

The slope of the $\frac{Z_{sol}im}{Z_{sol}real}$ relative to W gives the $R_{sol}C_{sol}$.

The slope of the $Z_{sol}im(1 + R_{sol}^2 W^2 C_{sol}^2)$ relative to W gives the $R_{sol}^2 C_{sol}$.

So we could extract the values of R_{sol} and C_{sol} for each solution in MATLAB by coding these equations.

Next step is to eliminate the effect of solution resistance. As shown in equivalent circuit model in **Fig 3.7** to obtain the complex double layer impedance Z_{dl} we should elicit the R_{sol} from the complex Z_x.

$$Z_x = Z_{dl} + R_{sol} \tag{3.15}$$

$$Z_{dl} = Z_x - R_{sol} \tag{3.16}$$

$$Z_m = \frac{Z_x Z_{sol}}{Z_x + Z_{sol}} \tag{3.17}$$

Measured impedance (Z_m) is a complex value (as explained in section 2.3.2) has real and imaginary parts.

$$Z_m = Z_{m(real)} + Z_{m(im)} \tag{3.18}$$

$$Z_{sol} = \frac{-j}{WC_{sol}} \tag{3.19}$$

$$Z_x = \frac{Z_m Z_{sol}}{Z_{sol} - Z_m} \tag{3.20}$$

$$Z_x = \frac{(Z_{m(real)} + Z_{m(im)})\frac{-j}{WC_{sol}}}{\frac{-j}{WC_{sol}} - (Z_{m(real)} + Z_{m(im)})} \tag{3.21}$$

$$Z_x = \frac{Z_{m(im)} - jZ_{m(real)}}{-j(1 + Z_{m(im)}WC_{sol}) - Z_{m(real)}WC_{sol}} \tag{3.22}$$

When the double layer impedance is acquired by eliminating the solution resistance, the double layer capacitance is found by processing impedance data at the low frequency range (double layer impedance is in short circuit at high frequencies).

We used the following formula at low frequency range to find C_{dl} in MATLAB.

$$C_{dl} = \frac{-j}{WC_{dl}} \tag{3.23}$$

$$Z_{dl} = \frac{C_{dl}R_t}{C_{dl} + R_t} \tag{3.24}$$

$$Z_{dl} = \frac{R_t}{R_t^2 W^2 C_{dl}^2 + 1} - j\frac{R_t^2 W C_{dl}}{R_t^2 W^2 C_{dl}^2 + 1} \tag{3.25}$$

In equation **3.25** the slope of the $\frac{1}{Zim}$ according to W gives C_{dl}.

As mentioned above, for condition that C_{dl} is equal to C (pure capacitor) and, the exponent, α is equal to 1 give the impedance of pure capacitor. So we should fit our extracted data to the equation below and we obtained α values.

$$CPE = \frac{1}{(C_{dl}jW)^{\alpha}} = \frac{1}{C_{dl}W^{\alpha}}(\cos(\frac{\prod \alpha}{2}) - j\sin(\frac{\prod \alpha}{2})) \tag{3.26}$$

Next step is to consider the resistance in the double layer impedance system (R_t). At this approximation we calculated the second approximation of double layer capacitance (C_0) and resistance in it.

$$\frac{1}{Z_m} = \frac{1}{R_t} + jWC_0 \tag{3.27}$$

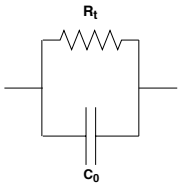

Figure 3.9 $R_t|C_0$

.

$$\frac{1}{Z_m} = \frac{1}{Z_{m(real)} + jZ_{m(im)}} = \frac{Z_{m(real)} - jZ_{m(im)}}{Z^2_{m(real)} + Z^2_{m(im)}} \tag{3.28}$$

$$\frac{1}{R_t} = \frac{Z_{m(real)}}{Z^2_{m(real)} + Z^2_{m(im)}} \tag{3.29}$$

$$R_t = \frac{Z^2_{m(real)} + Z^2_{m(im)}}{Z_{m(real)}} \tag{3.30}$$

The slope of the WC_0 relative to the will give the C_0.

$$WC_0 = \frac{Z_{m(im)}}{Z^2_{m(real)} + Z^2_{m(im)}} \tag{3.31}$$

3.4 Nyquist plots

In typical Nyquist plots real part and imaginary parts of impedance are represented as Z' and Z" in x and y axis, respectively. Z-F results are shown in these plots. High frequency side is shown in the left side and as we proceed the right side a semicircle which is followed by straight line indicates capacitive behavior.

For the first time in this work, we have plotted Z-V measurements in the Nyquist plot format. After solution resistance and capacitance effects are eliminated from the the Z-V measurements (impedance-phase-voltage), Nyquist plots were obtained in MATLAB by plotting real and imaginary part of the measured impedance for each bias voltage point. Z-V impedance measurements were conducted at 20 Hz constant frequency and swept from -1 to +1 bias voltage (10 mV AC signal).

4. EXPERIMENTAL RESULTS

Experimental results include numerical values of extracted R_{sol}, C_{sol}, C_{dl}, α, R_t and C_0 in the tables from Z-F plots. Nyquist plots which were obtained from the Z-F and Z-V measurements are given.

Nyquist plots for salt and pH solutions were acquired from both Z-V and Z-F results. The characteristic of each Z-F graphs for each molarity exhibitied the expected patterns with respect to electrochemical principles. On the other hand, Z-V Nyquist plots has showed distinct and roughly unique patterns for each salt solutions.

4.1 Experimental results for salt solutions

According to measurements acquired from LiCl solution showed that the electrical double layer values of increases as solution molarity increases.

Table 4.1
Experimental results for LiCl.

$I_0(LiCl)(M)$	$R_{sol}(\Omega)$	$C_{sol}(F)$	$C_{dl}(F)$	α	$R_t(\Omega)$	$C_0(F)$
0,001	4,00E+03	2,50E-11	1,00E-07	0,77	3,30E+04	1,00E-07
0,002	1,75E+03	2,29E-11	1,80E-07	0,74	3,20E+04	1,00E-07
0,005	6,00E+02	1,67E-11	2,20E-07	0,78	1,40E+04	1,00E-07
0,01	3,33E+02	1,80E-11	2,60E-07	0,79	1,00E+03	2,00E-07
0,025	1,50E+02	1,33E-11	2,70E-07	0,79	2,50E+03	2,00E-07
0,05	1,00E+02	1,50E-11	3,00E-07	0,79	1,50E+03	2,00E-07
0,1	3,33E+01	1,80E-11	3,30E-07	0,79	3,50E+03	2,00E-07

According to measurements acquired from NaCl solution showed that the electrical double layer values increases as solution molarity increases.

Table 4.2
Experimental results for NaCl.

$I_0(NaCl)(M)$	$R_{sol}(\Omega)$	$C_{sol}(F)$	$C_{dl}(F)$	α	$R_t(\Omega)$	$C_0(F)$
0,001	1,67E+03	3,60E-11	2,00E-07	0,76	3,30E+04	1,00E-07
0,002	1,00E+03	2,00E-11	3,00E-07	0,76	6,50E+03	2,00E-07
0,005	5,00E+02	2,00E-11	3,30E-07	0,77	8,50E+03	2,00E-07
0,01	2,00E+02	2,50E-11	3,50E-07	0,78	1,00E+03	2,00E-07
0,025	1,00E+02	2,00E-11	3,60E-07	0,74	6,67E+02	3,00E-07
0,05	9,00E+01	1,11E-11	3,80E-07	0,74	3,00E+03	2,00E-07
0,1	4,00E+01	1,25E-11	4,00E-07	0,75	2,00E+03	3,00E-07

According to measurements acquired from KCl solution showed that the electrical double layer values increases as solution molarity increases.

Table 4.3
Experimental results for KCl.

$I_0(KCl)(M)$	$R_{sol}(\Omega)$	$C_{sol}(F)$	$C_{dl}(F)$	α	$R_t(\Omega)$	$C_0(F)$
0,001	2,00E+03	2,50E-11	1,00E-07	0,77	1,40E+04	1,00E-07
0,002	1,33E+03	2,25E-11	1,40E-07	0,72	8,00E+03	1,00E-07
0,005	4,00E+02	2,50E-11	1,60E-07	0,75	6,00E+03	1,00E-07
0,01	2,00E+02	2,50E-11	1,80E-07	0,74	5,00E+03	1,00E-07
0,025	1,00E+02	2,00E-11	2,20E-07	0,73	2,00E+03	2,00E-07
0,05	7,00E+01	1,43E-11	2,50E-07	0,77	1,50E+03	2,00E-07
0,1	4,00E+01	1,25E-11	3,00E-07	0,76	1,00E+03	2,00E-07

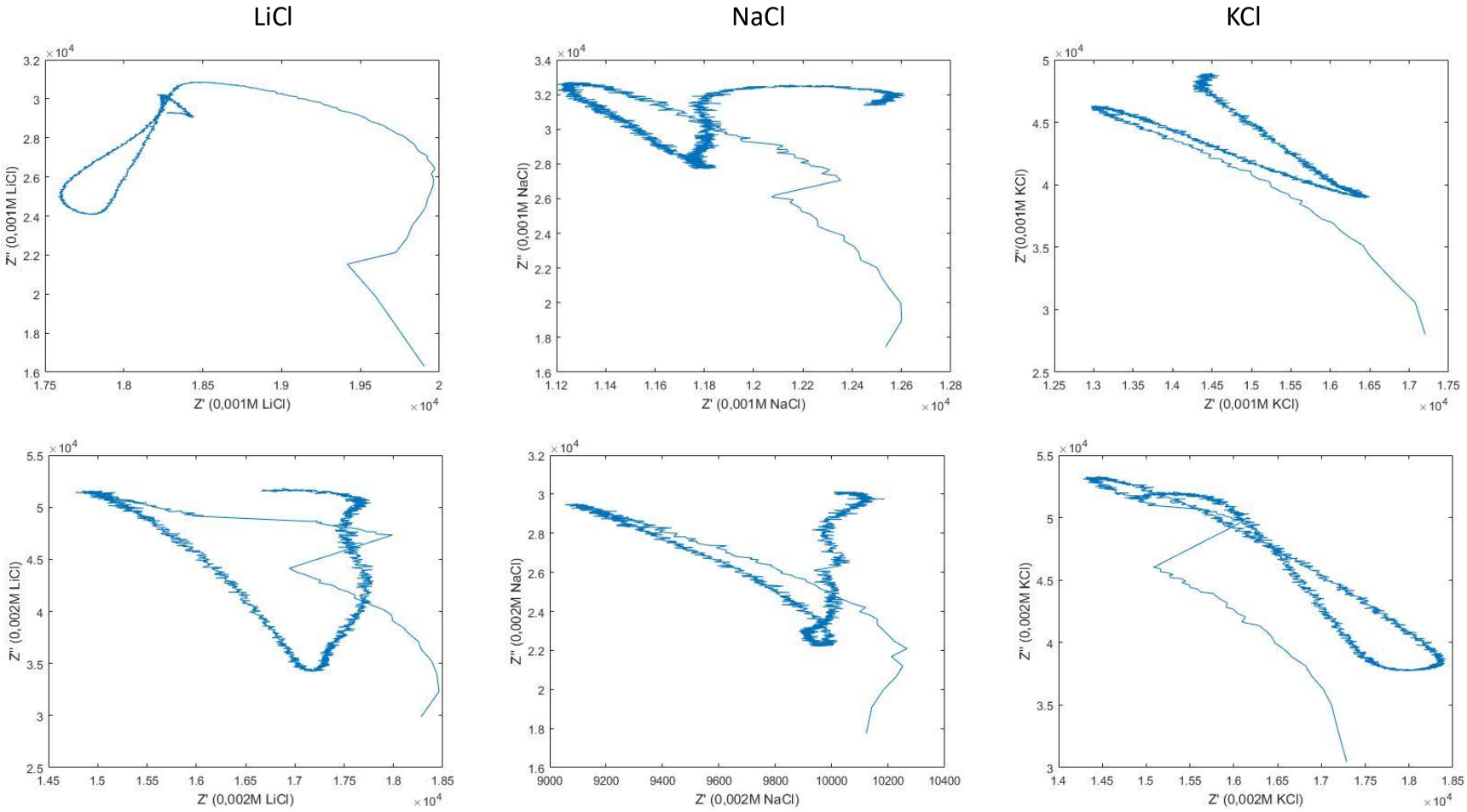

Figure 4.1 Nyquist plots of LiCl, NaCl and KCl (Z-V) for 0.001 M and 0.002 M.

.

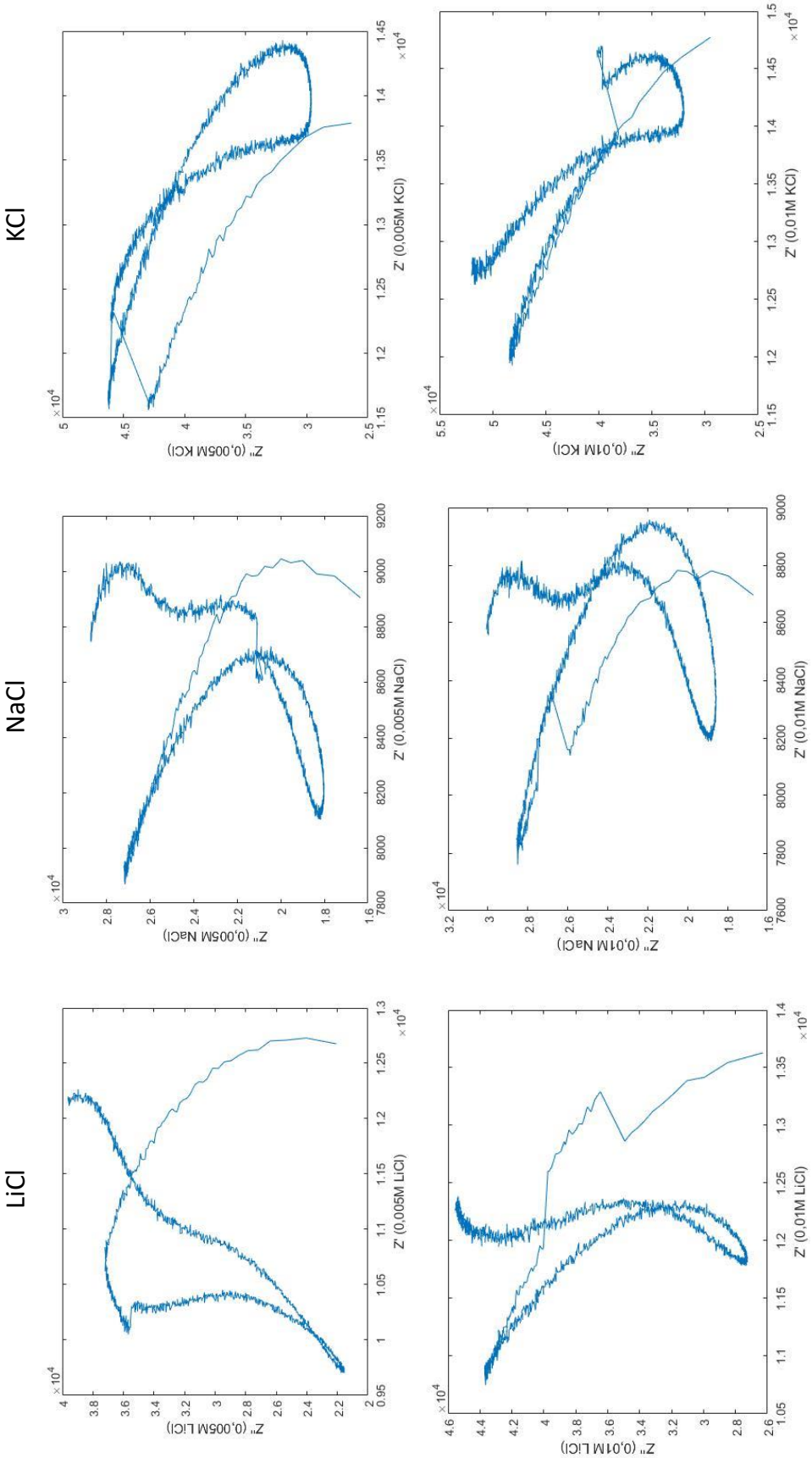

Figure 4.2 Nyquist plots of LiCl, NaCl and KCl (Z-V) for 0.005 M and 0.01 M.

.

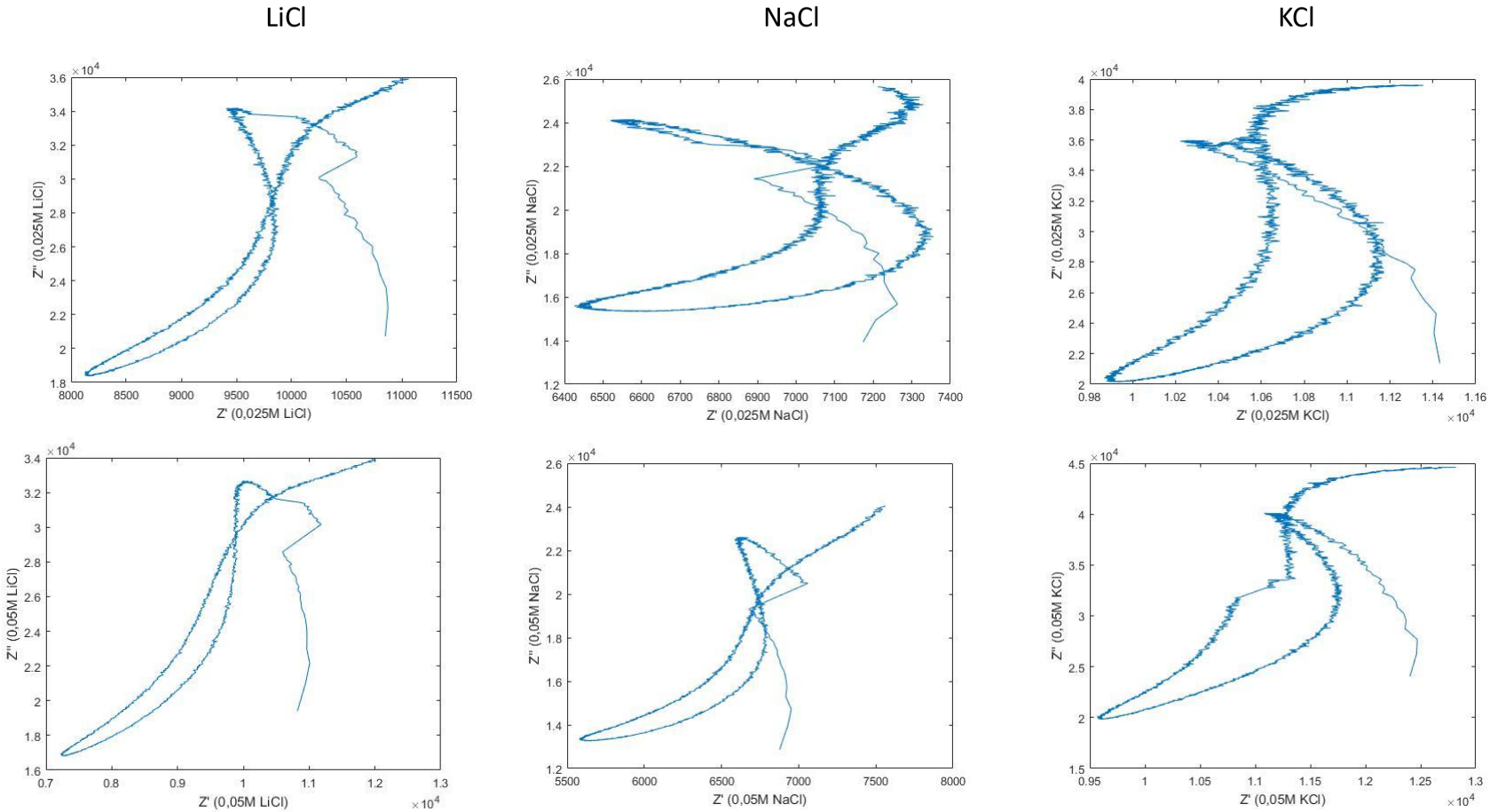

Figure 4.3 Nyquist plots of LiCl, NaCl and KCl (Z-V) for 0.025 M and 0.05 M.

.

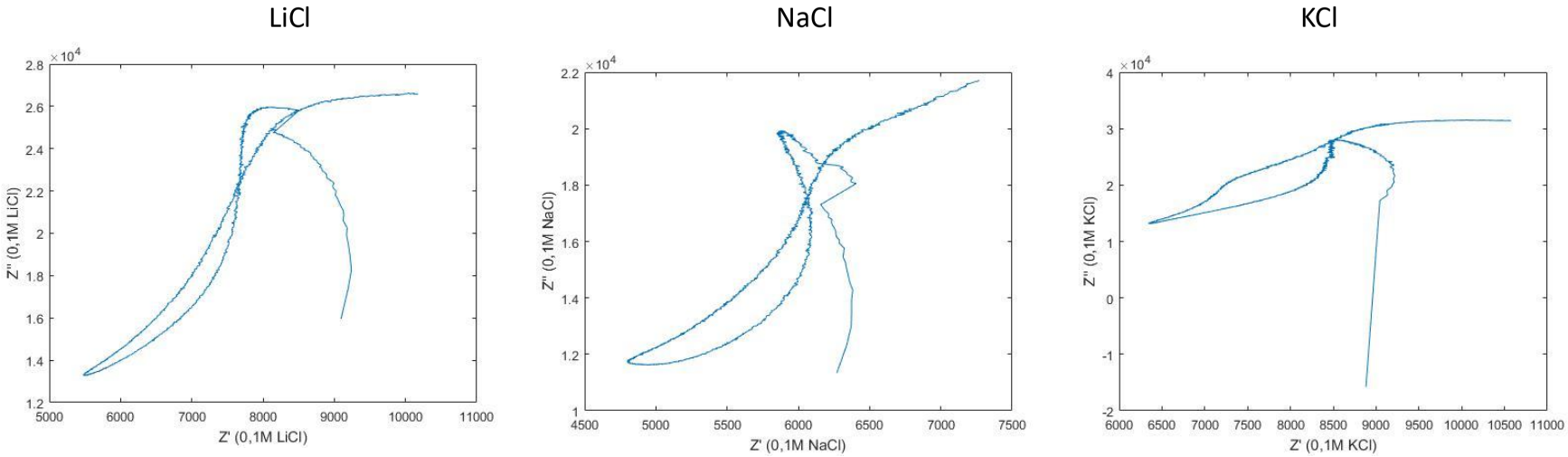

Figure 4.4 Nyquist plots of LiCl, NaCl and KCl (Z-V) for 0.1 M.

.

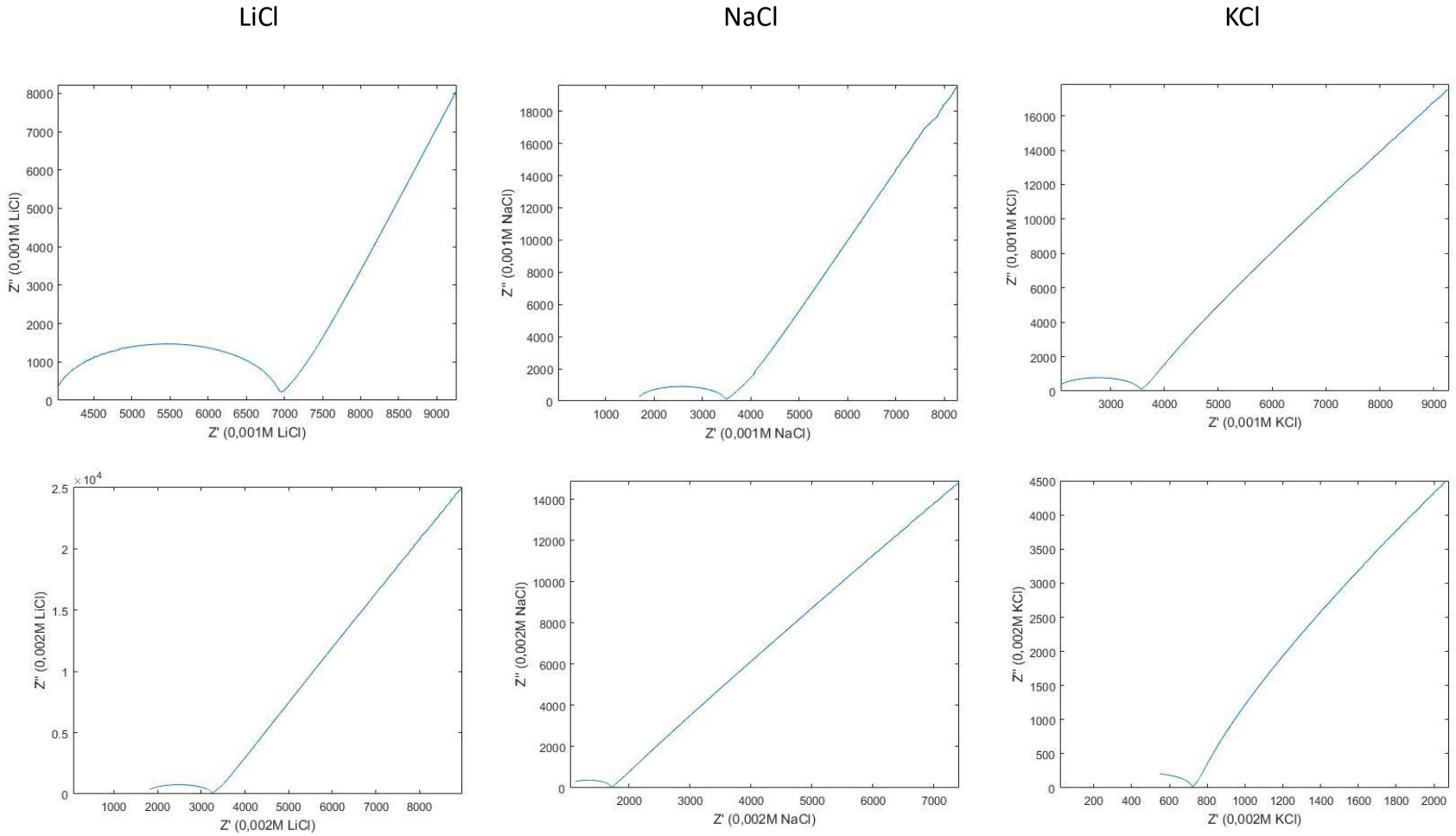

Figure 4.5 Nyquist plots of LiCl, NaCl and KCl (Z-F) for 0.001 M and 0.002 M.

.

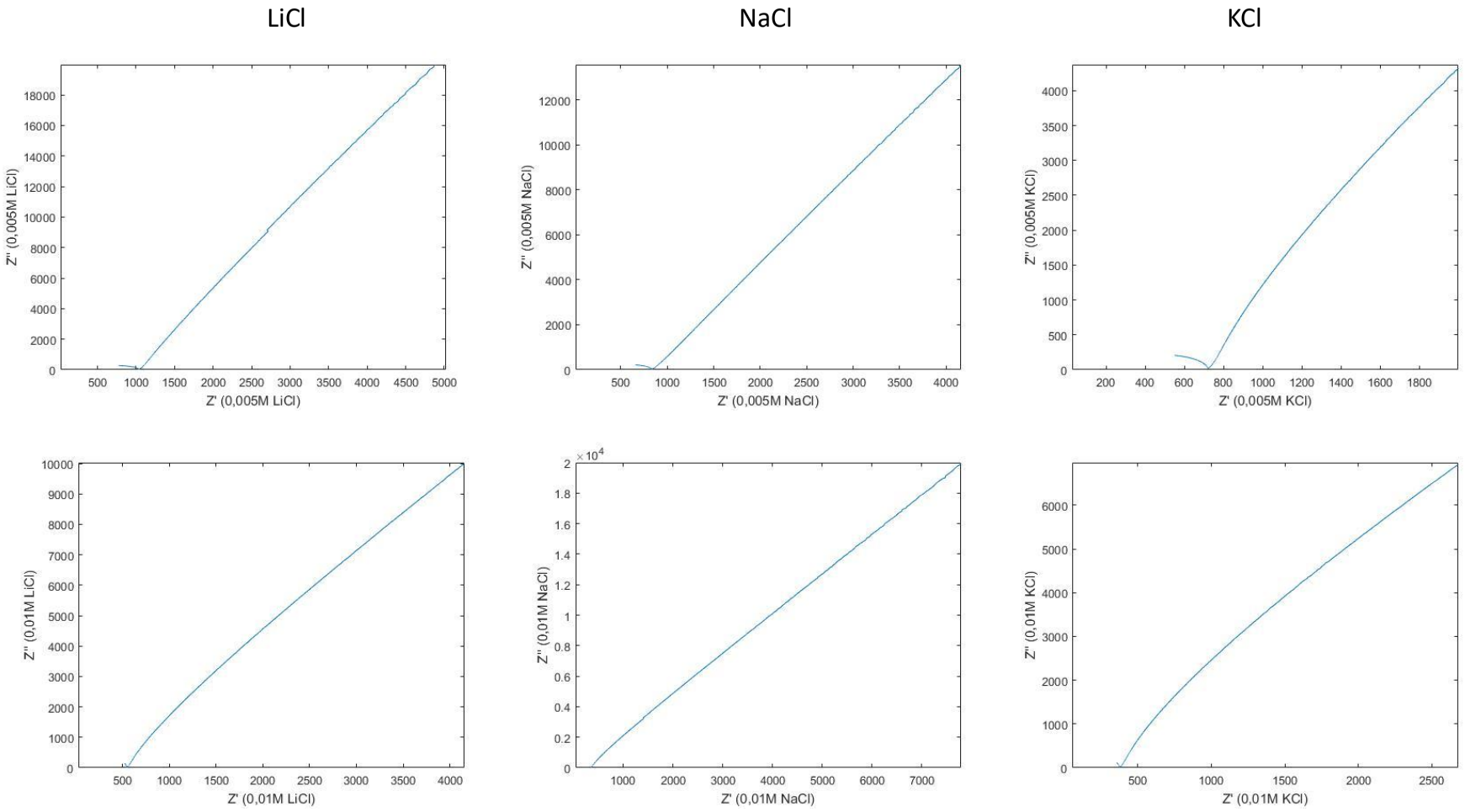

Figure 4.6 Nyquist plots of LiCl, NaCl and KCl (Z-F) for 0.005 M and 0.01 M.

.

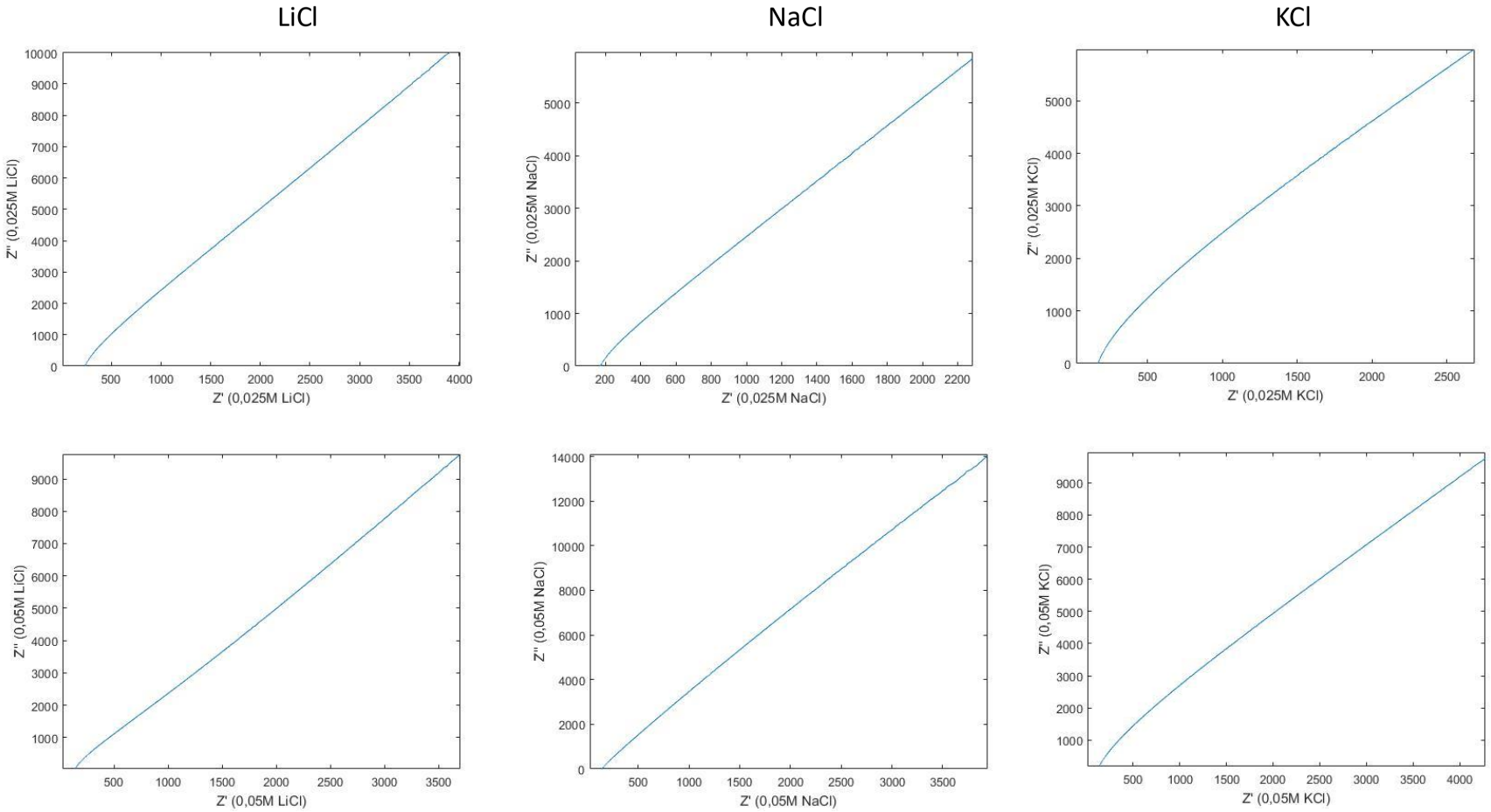

Figure 4.7 Nyquist plots of LiCl, NaCl and KCl (Z-F) for 0.025 M and 0.05 M.

.

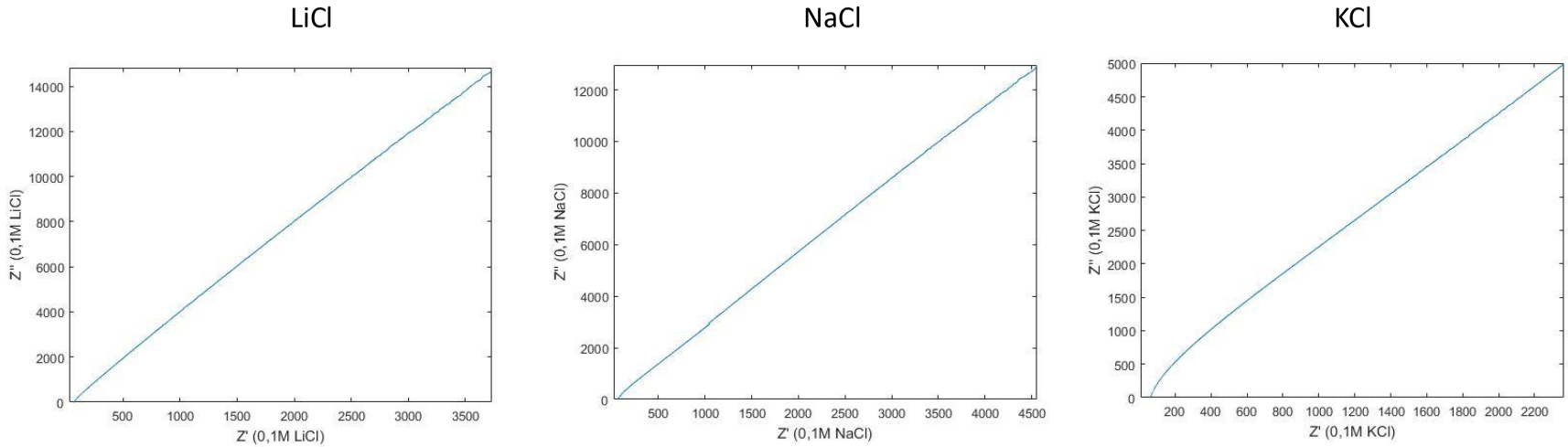

Figure 4.8 Nyquist plots of LiCl, NaCl and KCl (Z-F) for 0.1 M.

.

4.2 Experimental results for pH solutions

Electrical double layer values acquired from different pH solutions can also be interpreted as the same with the salt solutions' results. According to measurements acquired from each pH solution showed that the electrical double layer values of increases as the solution molarity increases for each pH solutions.

Table 4.4
Experimental results for pH 2.

$I_0(pH2)(M)$	$R_{sol}(\Omega)$	$C_{sol}(F)$	$C_{dl}(F)$	α	$R_t(\Omega)$	$C_0(F)$
0,001	1666,6	1,80E-11	1,50E-07	0,74	7000	2,00E-07
0,01	250	1,60E-11	2,00E-07	0,75	3000	2,00E-07
0,05	70	1,40E-11	3,00E-07	0,76	4500	2,00E-07
0,1	50	1,20E-11	4,00E-07	0,74	9500	2,00E-07

Table 4.5
Experimental results for pH 3.

$I_0(pH3)(M)$	$R_{sol}(\Omega)$	$C_{sol}(F)$	$C_{dl}(F)$	α	$R_t(\Omega)$	$C_0(F)$
0,001	1333,3	2,25E-11	3,00E-07	0,75	8000	2,00E-07
0,01	250	2,13E-11	3,50E-07	0,75	7500	2,00E-07
0,05	75	1,06E-11	4,00E-07	0,75	1000	4,00E-07
0,1	50	1,60E-11	4,50E-07	0,75	5250	4,00E-07

Table 4.6
Experimental results for pH 4.

$I_0(pH4)(M)$	$R_{sol}(\Omega)$	$C_{sol}(F)$	$C_{dl}(F)$	α	$R_t(\Omega)$	$C_0(F)$
0,001	1600	3,13E-11	2,00E-07	0,76	15000	1,00E-07
0,01	200	2,5E-11	2,50E-07	0,74	3000	2,00E-07
0,05	100	1E-11	3,00E-07	0,75	7000	2,00E-07
0,1	57,14	1,22E-11	3,50E-07	0,77	9000	2,00E-07

Table 4.7
Experimental results for pH 5.

$I_0(pH5)(M)$	$R_{sol}(\Omega)$	$C_{sol}(F)$	$C_{dl}(F)$	α	$R_t(\Omega)$	$C_0(F)$
0,001	1666,6	3,60E-11	2,00E-07	0,72	16000	1,00E-07
0,01	285	2,45E-11	2,50E-07	0,77	3000	2,00E-07
0,05	100	2,00E-11	2,70E-07	0,78	1000	2,00E-07
0,1	40	1,25E-11	3,00E-07	0,76	2666,6	3,00E-07

Table 4.8
Experimental results for pH 6.

$I_0(pH6)(M)$	$R_{sol}(\Omega)$	$C_{sol}(F)$	$C_{dl}(F)$	α	$R_t(\Omega)$	$C_0(F)$
0,001	1800	2,78E-11	1,00E-07	0,77	33000	1,00E-07
0,01	200	2,50E-11	3,00E-07	0,77	4000	2,00E-07
0,05	100	1,00E-11	4,00E-07	0,76	2000	3,00E-07
0,1	33,3	1,80E-11	4,50E-07	0,77	1333,3	3,00E-07

Table 4.9
Experimental results for pH 7.

$I_0(pH7)(M)$	$R_{sol}(\Omega)$	$C_{sol}(F)$	$C_{dl}(F)$	α	$R_t(\Omega)$	$C_0(F)$
0,001	1666,6	3,60E-11	2,00E-07	0,76	33000	1,00E-07
0,01	200	2,50E-11	3,50E-07	0,78	1000	2,00E-07
0,05	90	1,10E-11	3,80E-07	0,74	3000	2,00E-07
0,1	40	1,25E-11	4,00E-07	0,75	2000	3,00E-07

Table 4.10
Experimental results for pH 8.

$I_0(pH8)(M)$	$R_{sol}(\Omega)$	$C_{sol}(F)$	$C_{dl}(F)$	α	$R_t(\Omega)$	$C_0(F)$
0,001	1750	2,28E-11	2,00E-07	0,77	10000	2,00E-07
0,01	333	1,80E-11	4,00E-07	0,76	6000	3,00E-07
0,05	150	1,33E-11	5,00E-07	0,75	2000	4,00E-07
0,1	40	1,25E-11	6,00E-07	0,76	3250	4,00E-07

Table 4.11
Experimental results for pH 9.

$I_0(pH9)(M)$	$R_{sol}(\Omega)$	$C_{sol}(F)$	$C_{dl}(F)$	α	$R_t(\Omega)$	$C_0(F)$
0,001	1666	3,60E-11	2,00E-07	0,72	10000	1,00E-07
0,01	166,6	3,60E-11	3,00E-07	0,73	5000	2,00E-07
0,05	100	1,00E-11	4,00E-07	0,73	2250	4,00E-07
0,1	75	1,06E-11	7,40E-07	0,77	1333,3	6,00E-07

Table 4.12
Experimental results for pH 11.50.

$I_0(pH11.50)(M)$	$R_{sol}(\Omega)$	$C_{sol}(F)$	$C_{dl}(F)$	α	$R_t(\Omega)$	$C_0(F)$
0,001	1500	1,33E-11	4,00E-07	0,76	8333,3	3,00E-07
0,01	250	1,60E-11	6,00E-07	0,74	5000	5,00E-07
0,05	150	1,33E-11	6,50E-07	0,78	5600	5,00E-07
0,1	100	1,00E-11	8,00E-07	0,75	2125	8,00E-07

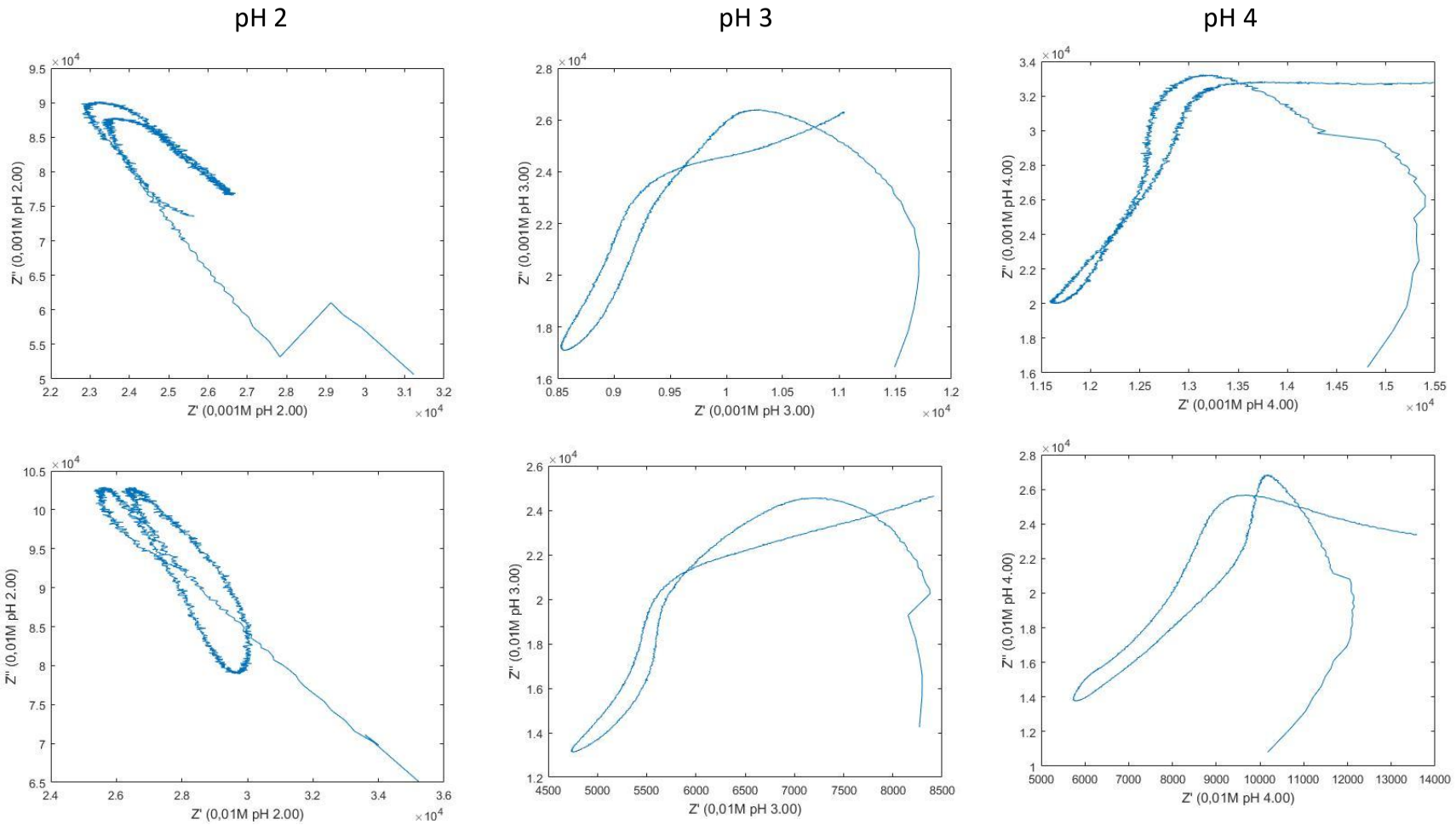

Figure 4.9 Nyquist plots of pH 2, pH 3 and pH 4 (Z-V) for 0.001 M and 0.01 M.

.

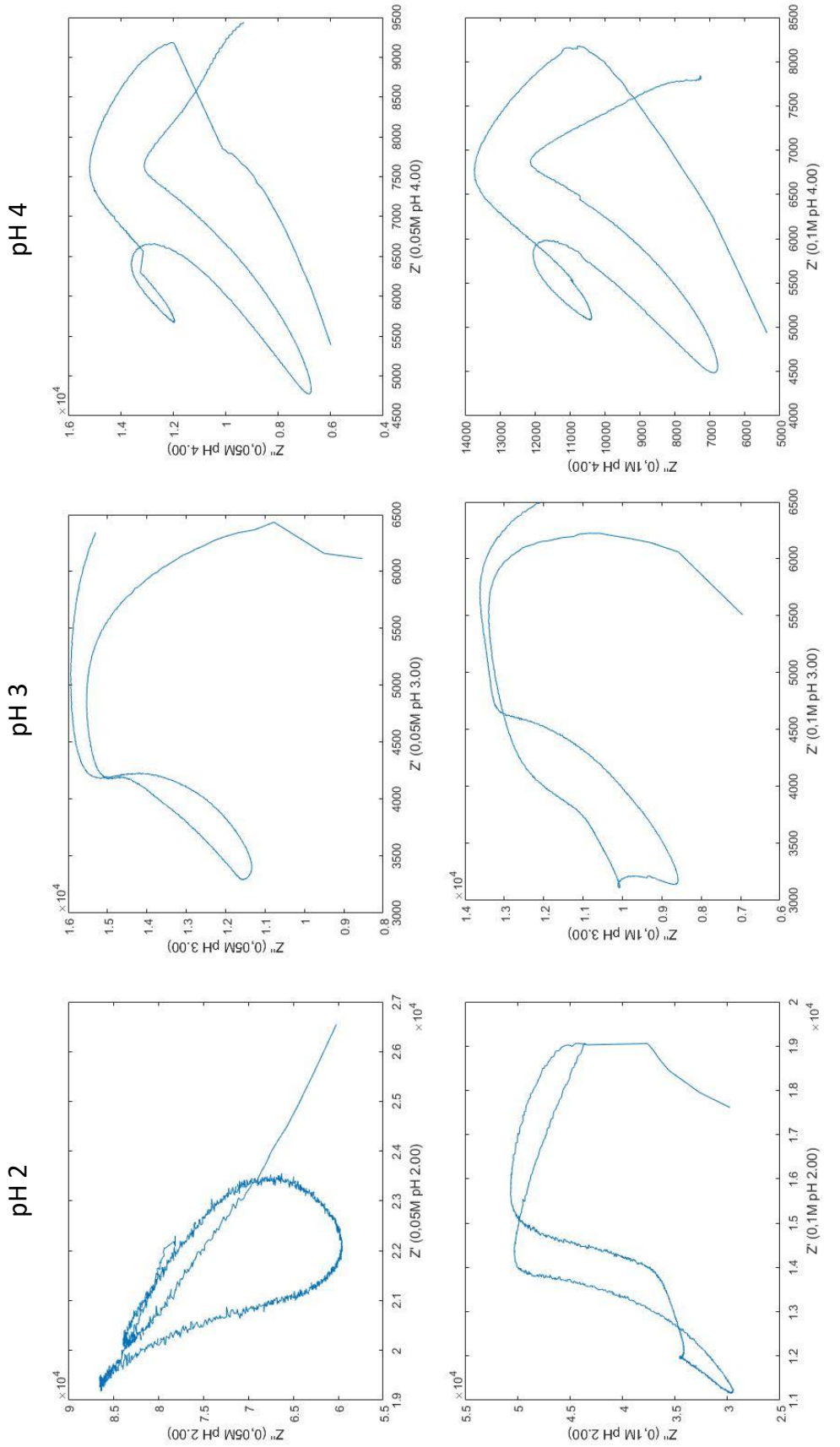

Figure 4.10 Nyquist plots of pH 2, pH 3 and pH 4 (Z-V) for 0.05 M and 0.1 M.

.

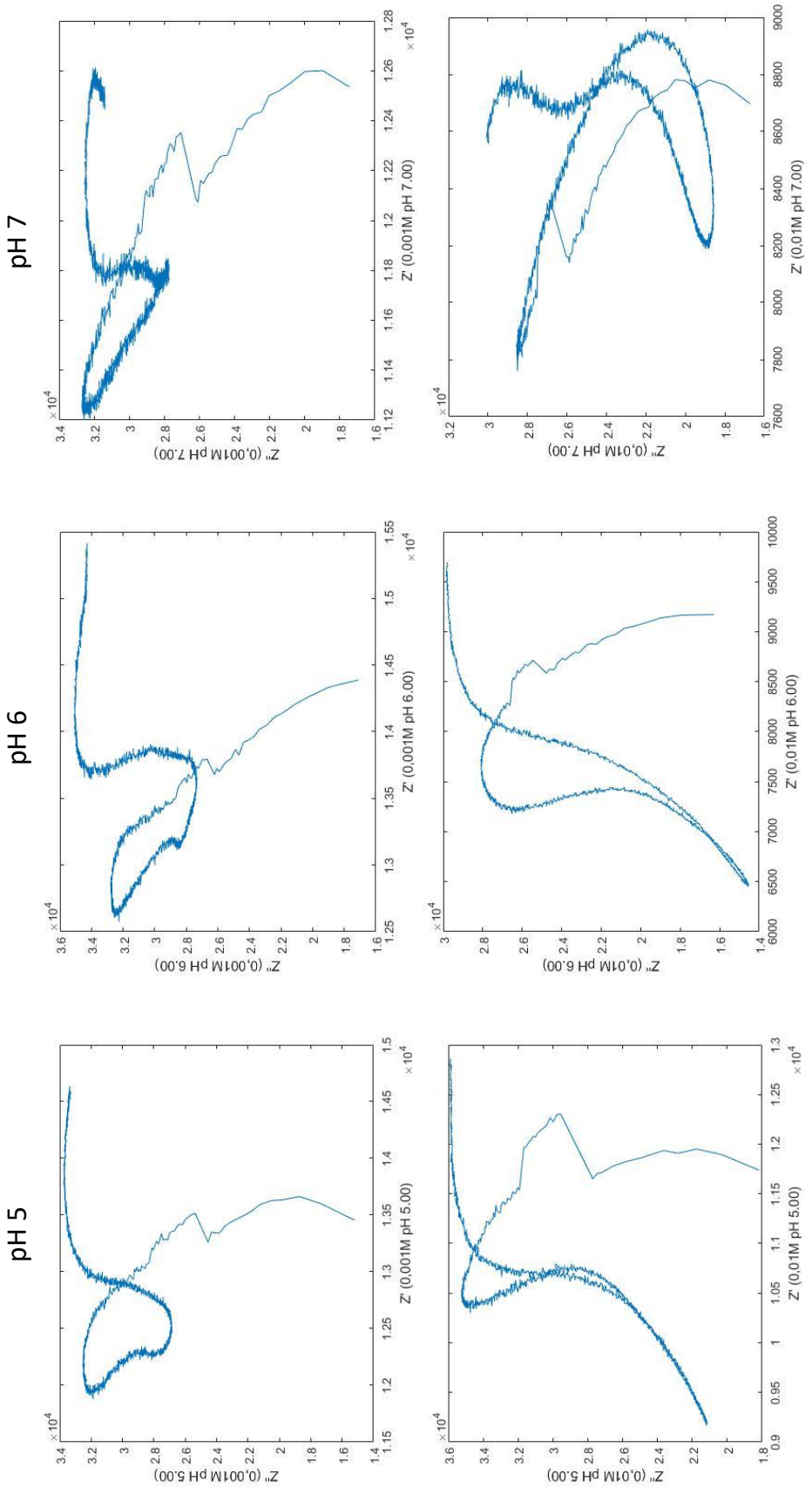

Figure 4.11 Nyquist plots of pH 5, pH 6 and pH 7 (Z-V) for 0.001 M and 0.01 M.

.

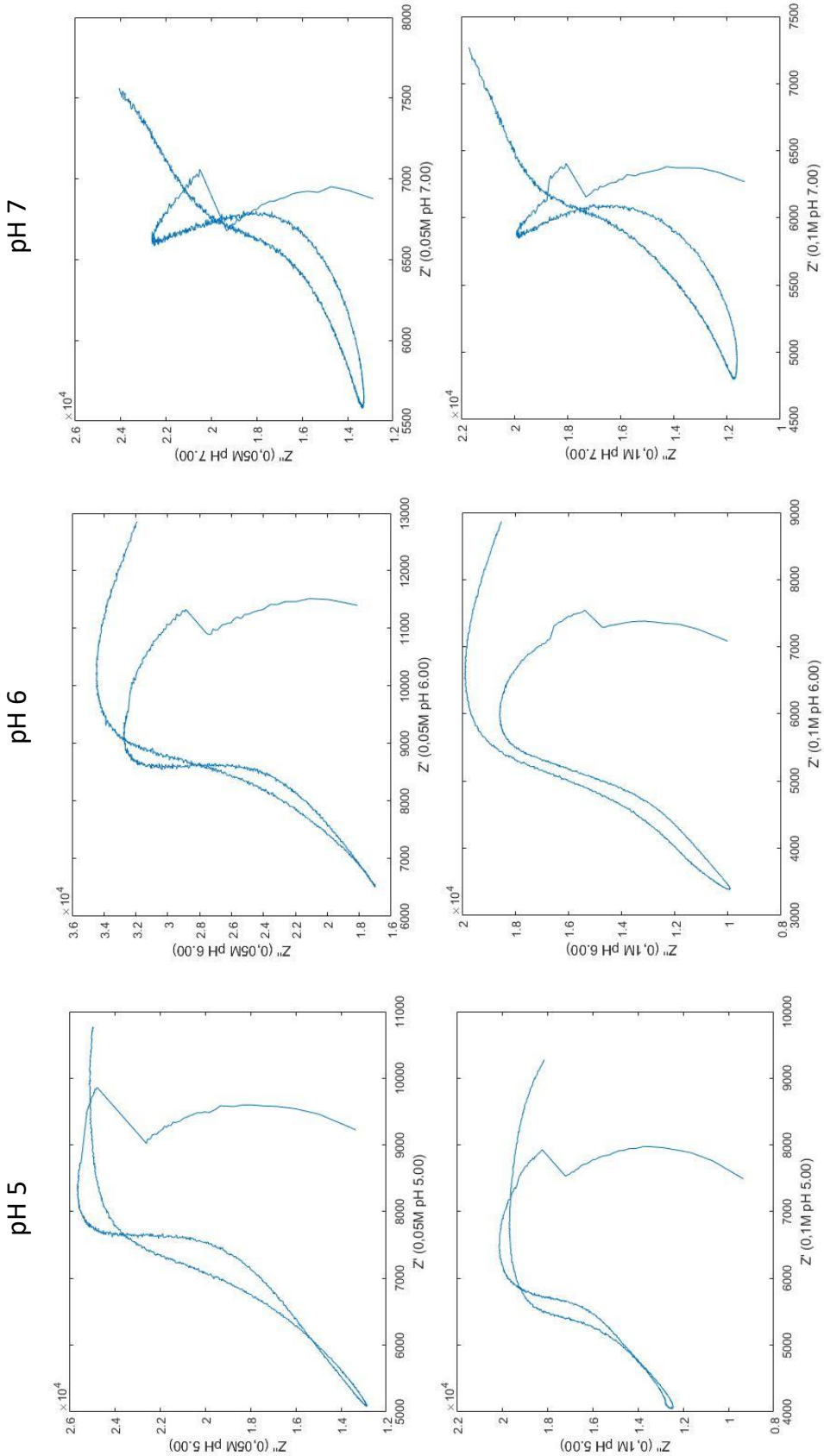

Figure 4.12 Nyquist plots of pH 5, pH 6 and pH 7 (Z-V) for 0.05 M and 0.1 M.

.

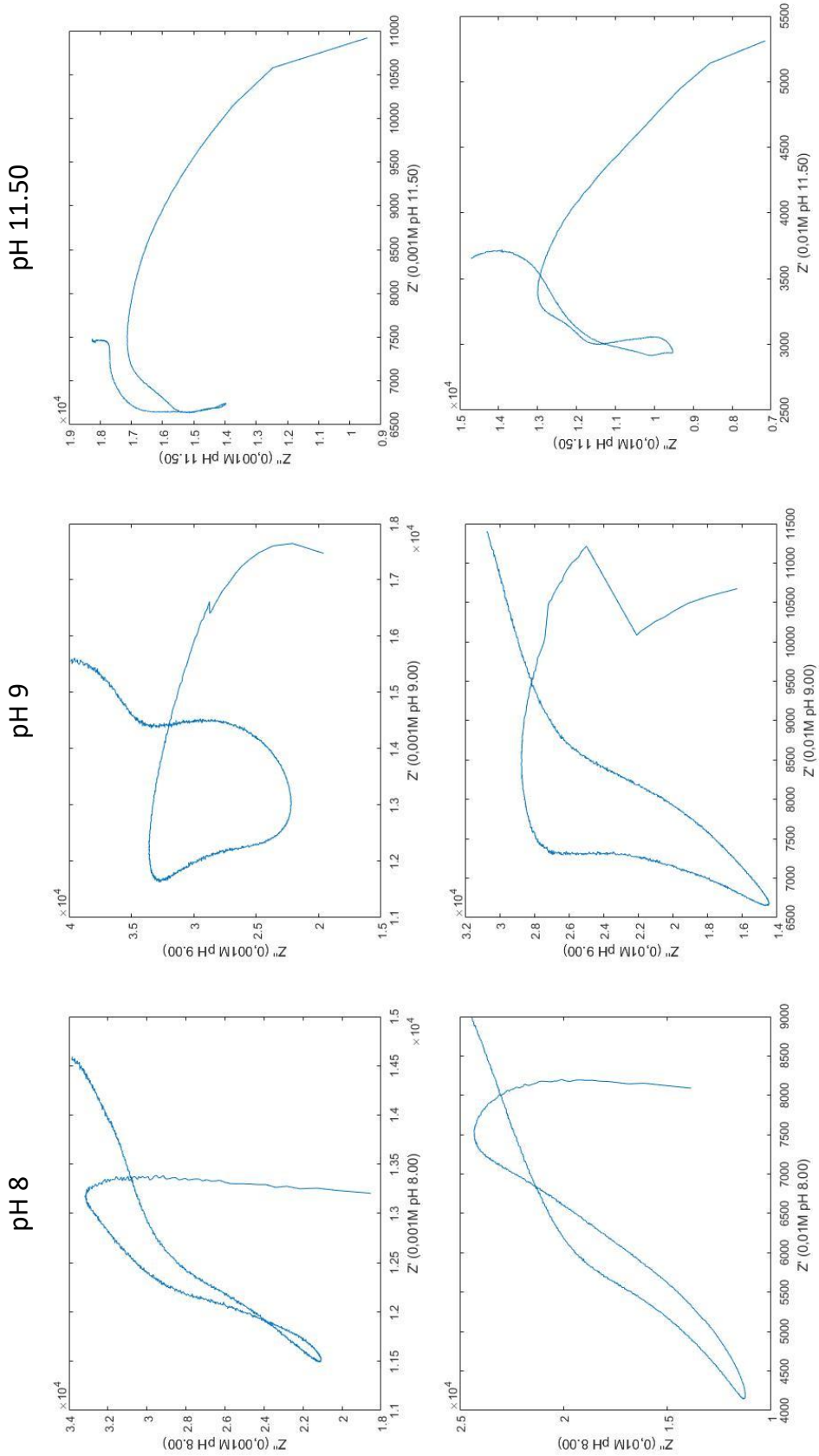

Figure 4.13 Nyquist plots of pH 8, pH 9 and pH 11.50 (Z-V) for 0.001 M and 0.01 M.

.

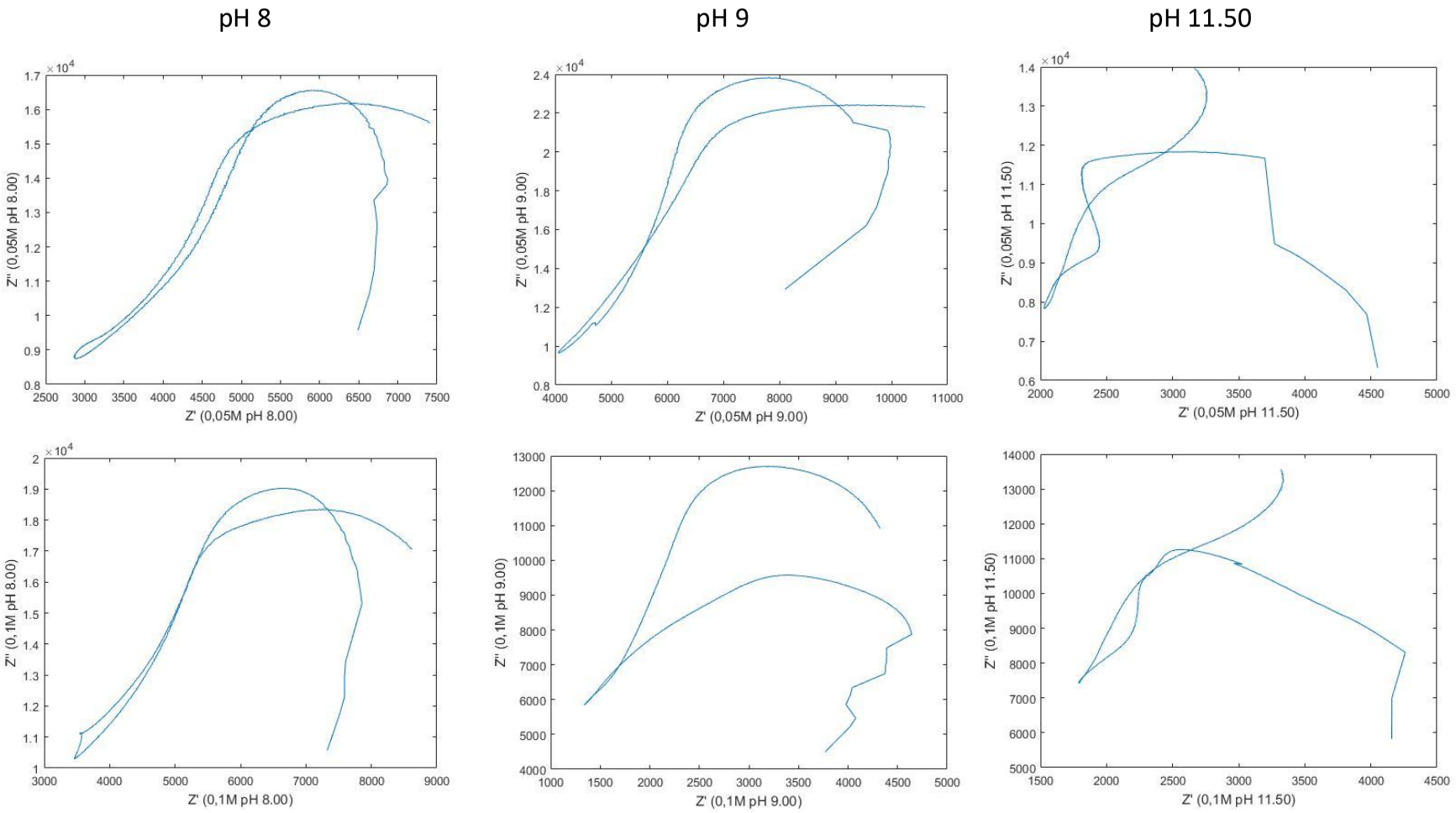

Figure 4.14 Nyquist plots of pH 8, pH 9 and pH 11.50 (Z-V) for 0.05 M and 0.1 M.

.

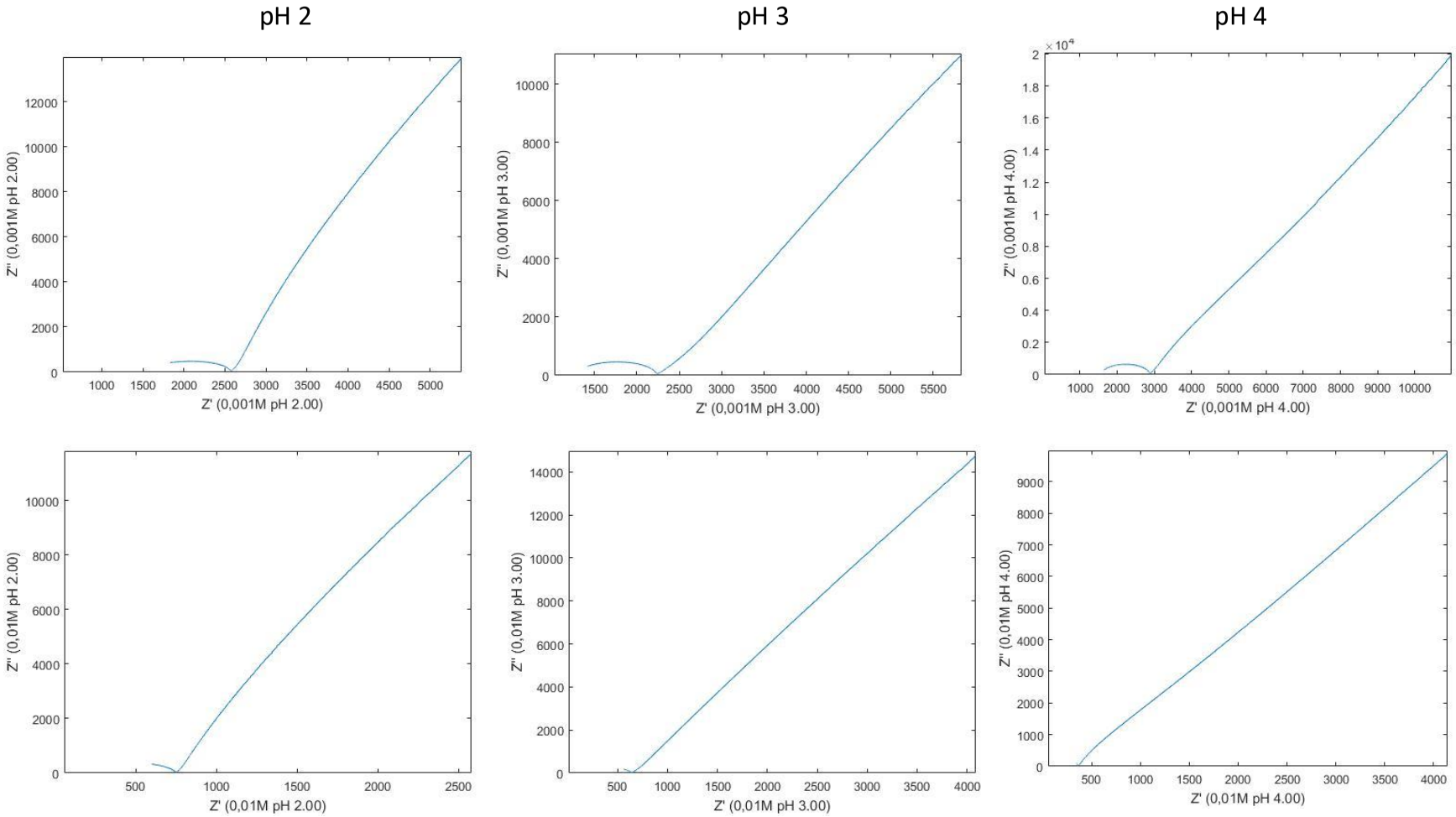

Figure 4.15 Nyquist plots of pH 2, pH 3 and pH 4 (Z-F) for 0.001 M and 0.01 M.

.

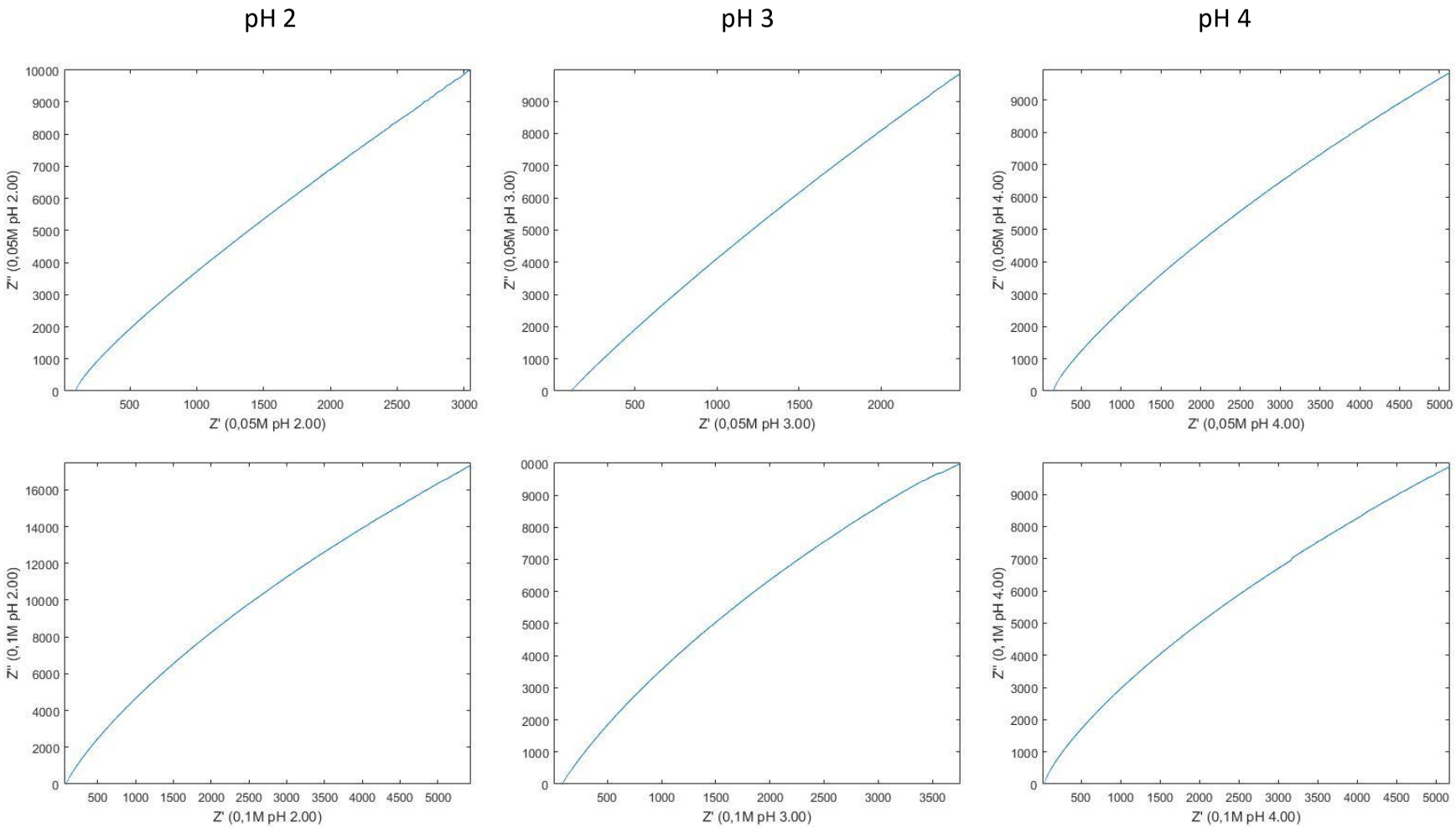

Figure 4.16 Nyquist plots of pH 2, pH 3 and pH 4 (Z-F) for 0.05 M and 0.1 M.

.

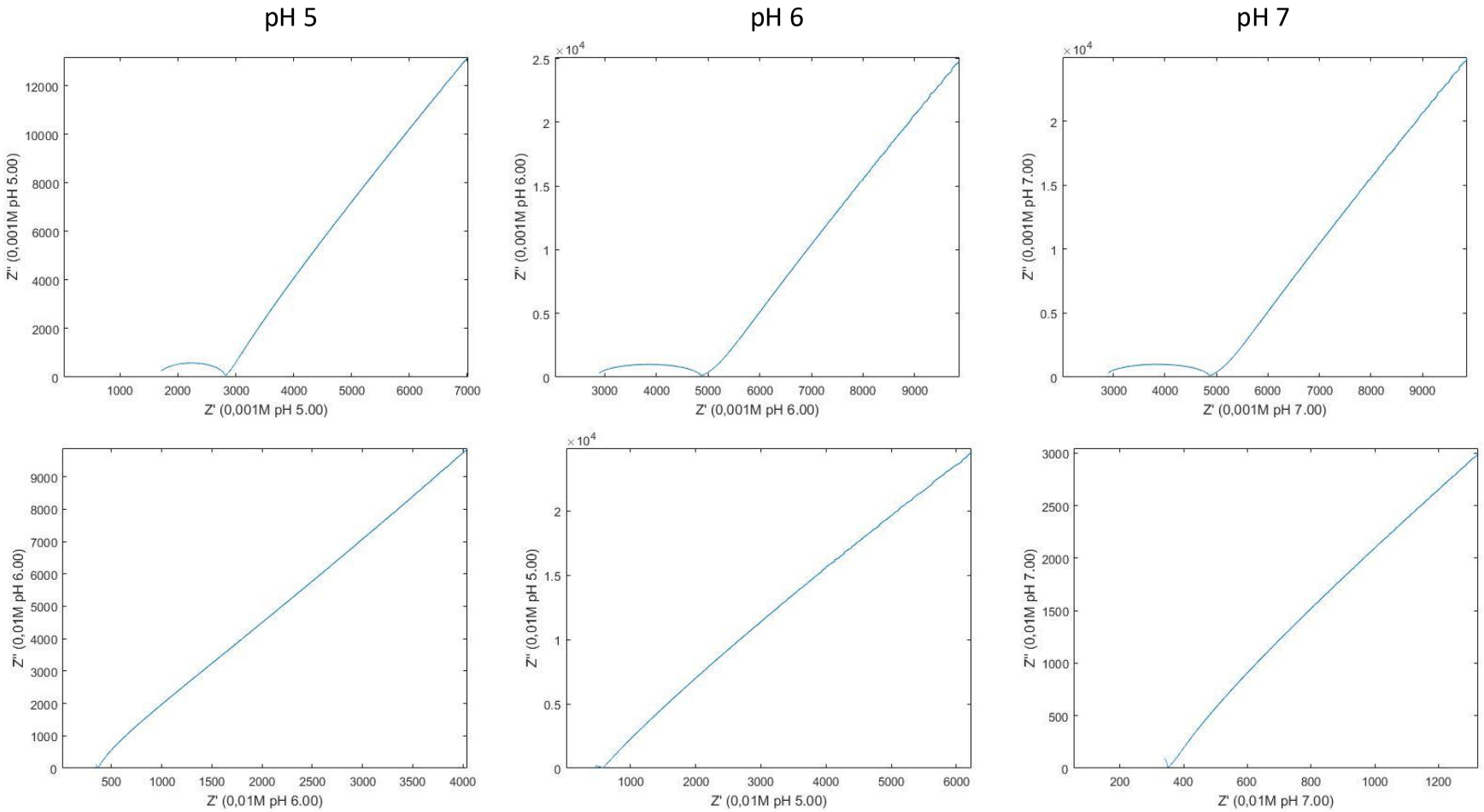

Figure 4.17 Nyquist plots of pH 5, pH 6 and pH 7 (Z-F) for 0.001 M and 0.01 M.

.

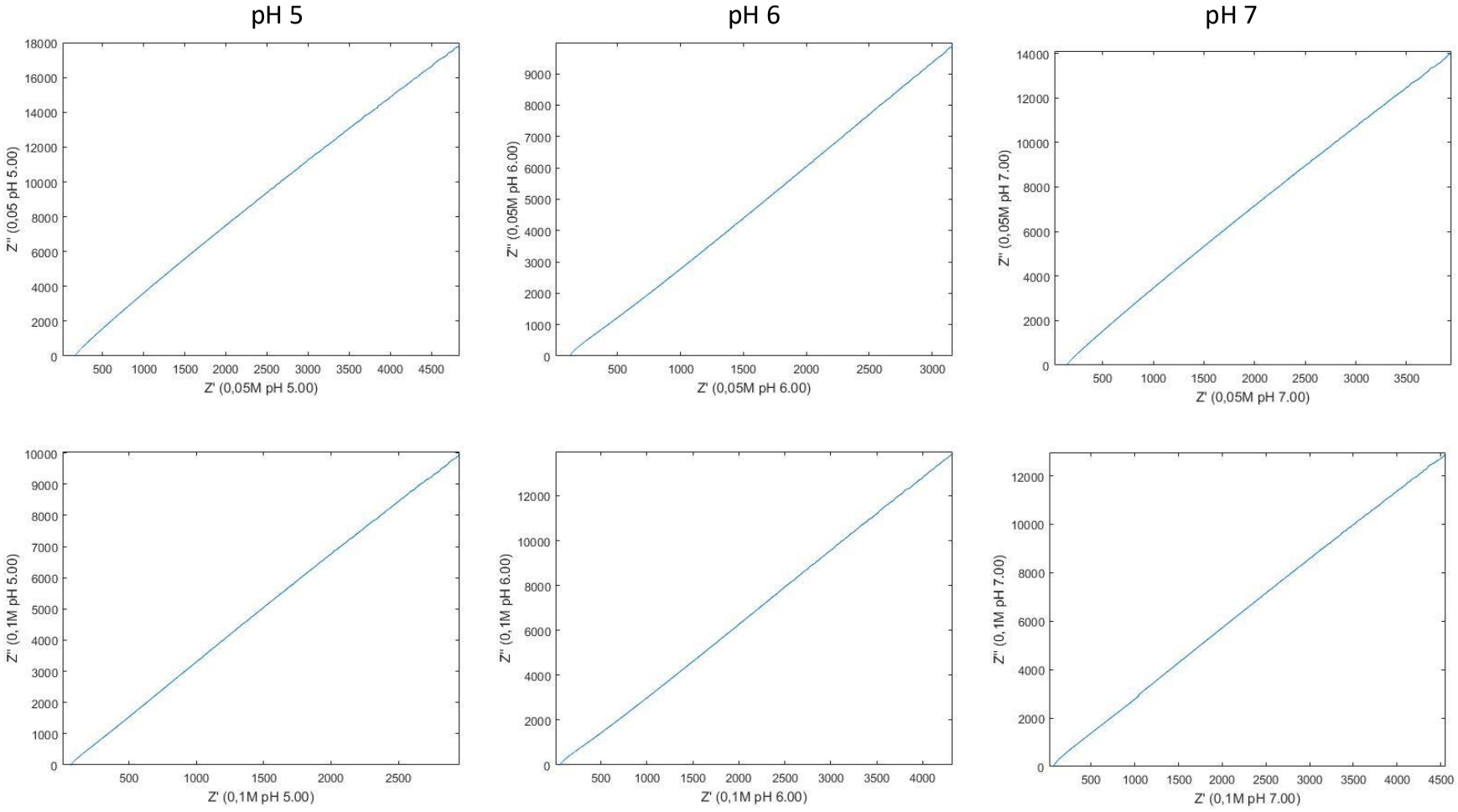

Figure 4.18 Nyquist plots of pH 5, pH 6 and pH 7 (Z-F) for 0.05 M and 0.1 M.

.

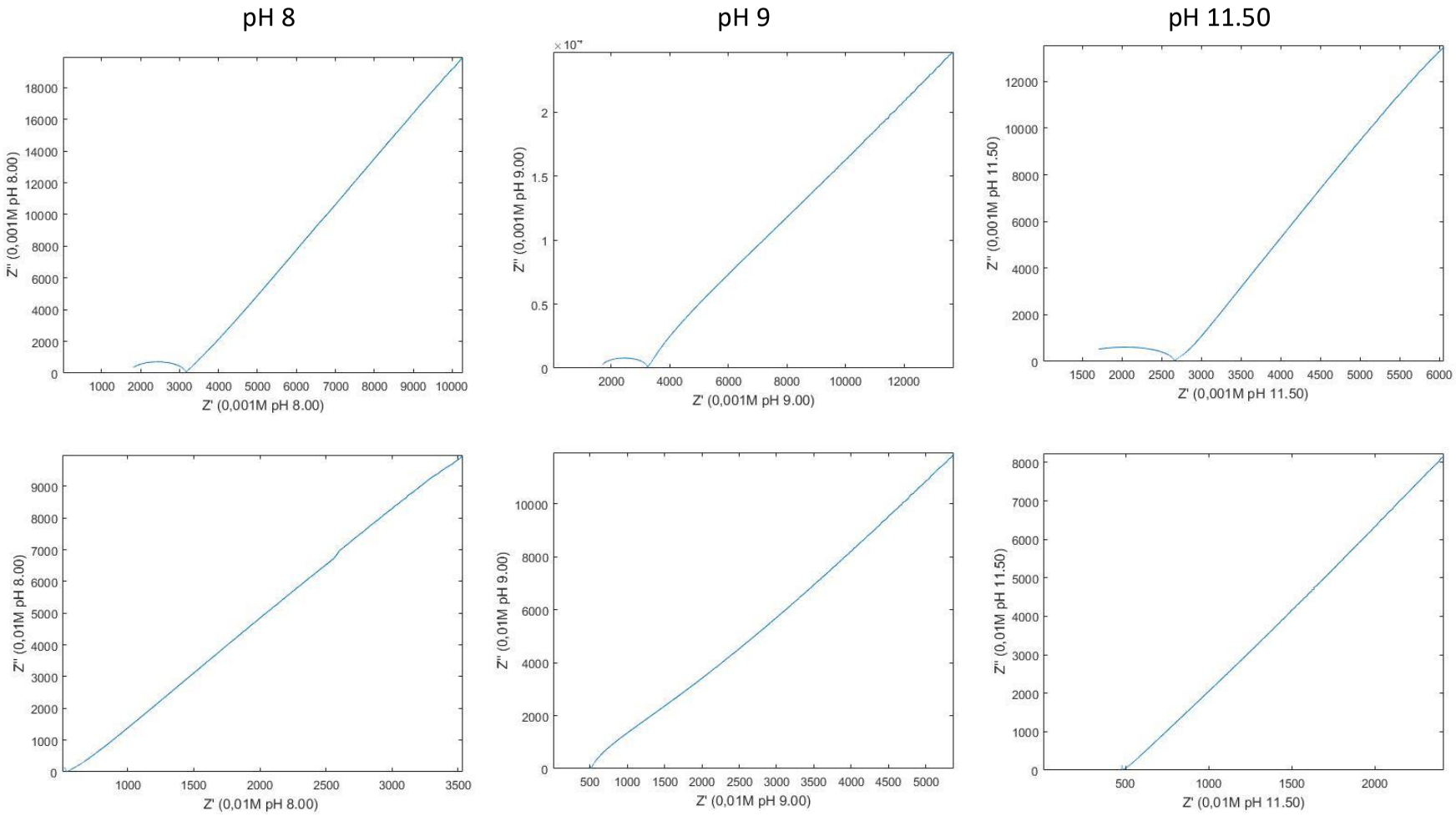

Figure 4.19 Nyquist plots of pH 8, pH 9 and pH 11.50 (Z-F) for 0.001 M and 0.01 M.

.

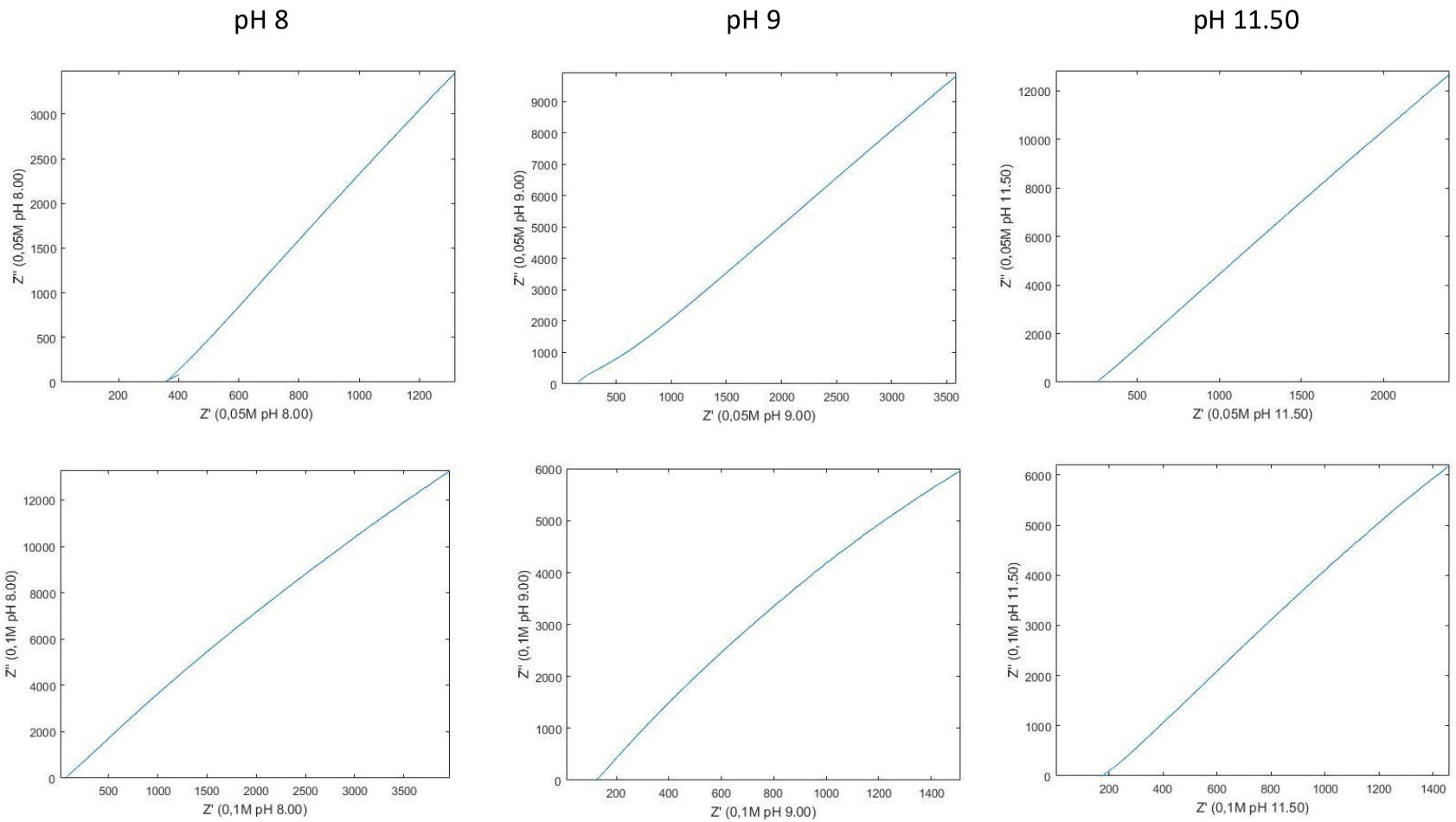

Figure 4.20 Nyquist plots of pH 8, pH 9 and pH 11.50 (Z-F) for 0.05 M and 0.1 M.

.

5. DISCUSSION

The need for high throughput, fast and low cost diagnosis have resulted in the emergence of POC technology. Many of the challenges in POC technology can be fulfilled by electronic microdevices which have contributed to miniaturization of tools and micro-fabrication processes [1] [2]. Microfabrication techniques have provided the construction of microelectromechanical systems (MEMS) which found many applications in the biomedical field, especially in the developments of sensors. MEMS can eliminate many error-causing processes and improve research capabilities. Microfluidics and solution based sensing applications are new research trends of MEMS [4]. BioMEMS have been advanced to characterize, monitor and detect analytes and biological fluids. For clinical diagnosis, the analysis of electrolytes such as sodium and potassium and the level of pH in the body fluids are significant parameters. Non-faradaic electrochemical impedimetric sensors are in this category where characterization methods can improve most biomedical applications. For these purposes, this study focused on the characterization of non-faradaic label free impedimetric electrochemical sensor.

Nevertheless, traditional technologies have mostly been conducted by the electrochemical impedance spectroscopy (EIS) that requires labeling such as special agents, redox reactions and also reference probes. In this study overall process was conducted as label free and without reactions (non-faradaic). Impedance measurements were conducted with Impedance Analyzer (E4990A). Different types of analyte solutions have been characterized to overwhelm this labeling challenge. Impedance measurement enables label-free operation since it does not depend on special agents as it mentioned in literature [4]. It is used in broad range of field as a powerful measurement technique by means of its ability to be quick-response, label-free by measuring the resistance and capacitance values of electrochemical system [1]. Moreover, impedance is a powerful analyzing method for the complex electrical resistance of a system and any bulk changes at the surface as label-free by measuring the resistance and capacitance values of electrochemical system which also makes it a very useful tool for the electrochemical

methods which makes it the potential tool for sensor design. Sensors are constructed to observe electrochemical changes at the surface of electrodes according to various analytes. For this reason, growing interest towards the development of impedimetric sensor is being accelerated. Impedimetric approaches have been applied to characterize the fabrication of the sensors and monitor the changes [5] on a variety of droplet-based analytes based on the electrical double layer. Therefore, in this study, electrical double layer capacitance values were extracted for each solution to characterize the sensor and enable to interpret molarity and EDL dependence of solution.

Electrical impedance is as a ratio of current change when a voltage is applied to the circuit. Thus, impedance of an electrode-solution is based on both frequency and bias and result in complex impedance value including phase and magnitude [4]. The principle of impedance measurements in this study was based on the wide range of frequency (20 Hz to 10 MHz) and potential (-1 V to +1 V) sweep set-up which provide a complex impedance consisting of real and imaginary parts (Z' and Z"). Most of the electrochemical studies use impedance results according to Nyquist plot which plots real and imaginary part of impedance. For the interpretation of impedance spectra, the convenient equivalent circuit model was set to acquire an accurate analysis and characterization compared to EIS which has default equivalent circuit model and gives electrical double layer capacitance values according to constant phase element, and the real and imaginary parts of complex impedance were obtained and Nyquist plots were plotted. However, in this study, we extracted double layer capacitance values our own regarding our circuit design. Results were evaluated according to both EDL values and Nyquist plots.

Results exhibited that the electrical double layer capacitance values of each solution increase, when their molarities increase. Although most of the electrochemical research has used Nyquist plots for impedance at different frequency sweep set up (Z-F) to interpret their experimental results, we plot Nyquist plots both for different frequency and voltage sweep set up (Z-F and Z-V). Results especially for Z-V showed that each solution has different patterns on Nyquist plots. Furthermore, a wide range of molarities for both salt and pH solutions provided a wider scope of characterization

of different analytes.

This should be highlighted as a future consideration that the longer operation time cause the droplet volume decrease that may result in drifts of results.

Furthermore, interdigitated electrode-based pH detection has been studied in the literature. Rajapaska et al. used AuIDE on Silicon substrate fabricated by conventional photolithography method and electrically characterized according to current-voltage (I-V) measurements in the presence of various pH solutions (pH range between 3 to 12) to test the applicability of the electrode as a chemical pH sensor [23], and Azmi et al. also studied the aluminum interdigitated electrodes (IDE) on a silicon substrate that is fabricated by conventional photolithography method for pH sensing. The IDE was fabricated using standard photolithography process and they obtained electrical characteristics from current-voltage curves [24]. Another study also proposed that the aluminum IDE electrode for pH sensing applications and conducted small range of pH solutions (pH 4– pH 7 – pH 10) and electrical characteristics have been done by capacitance values of pH solutions [25]. However, according to these studies conducted with similar approaches, results were only evaluated by I-V curves which may result in many limited findings in terms of differentiation of different pH solutions as shown in Figure 1.3 which shows the I-V patterns of different pH solutions and there are overlapped patterns. Additionally, the other studies only used three different pH solution to characterize the sensor and measurements were conducted at Aluminum IDE which could restricts the voltage range operation of the DUT to avoid reactions on the electrode surface.

The other important point that should be highlighted is the relationship between impedance and pH in biomedical field. Impedance and pH monitoring have been used in diagnosis of reflux in clinics. However, procedure has been conducted with two catheters for both pH and impedance. Unquestionably, impedance tracing combined with pH in the same catheter may be the future need to overwhelm the clinical outcomes. This study may be the idea for the interpretation of pH with impedance results due to results showed different results for different pH solutions.

6. CONCLUSION AND FUTURE WORK

In conclusion, these results will lead to label free measurement of analyte type, concentration and pH values upon data processing of multiple reference and analyte measurements and results will be a base for data processing applications for future research. Big data and deep learning methods such as clustering, regression or classification can be used to build predictive models and identify different salt types, concentrations and pH values.

REFERENCES

1. Demirok, U. K., A. Verma, and J. T. L. Belle, "The development of a label-free electrochemical impedance based pointof-care technology for multimarker detection," *Journal of Biosensors Bioelectronics*, Vol. S12, Jun 2013.

2. Chin, C. D., S. Y. Chin, T. Laksanasopin, and S. K. Sia, "Low-cost microdevices for point-of-care testing," *Point-of-Care Diagnostics on a Chip Biological and Medical Physics, Biomedical Engineering*, p. 3–21, Dec 2012.

3. Han, L., P. Liu, V. A. Petrenko, and A. Liu, "A label-free electrochemical impedance cytosensor based on specific peptide-fused phage selected from landscape phage library," *Scientific Reports*, Vol. 6, no. 1, 2016.

4. Daniels, J. S., and N. Pourmand, "Label-free impedance biosensors: Opportunities and challenges," *Electroanalysis*, Vol. 19, no. 12, p. 1239–1257, 2007.

5. Guan, J.-G., Y.-Q. Miao, and Q.-J. Zhang, "Impedimetric biosensors," *Journal of Bioscience and Bioengineering*, Vol. 97, no. 4, p. 219–226, 2004.

6. Selvam, A. P., K. M. Vattipalli, and S. Prasad, "Design of a high sensitive non-faradaic impedimetric sensor," *2012 Annual International Conference of the IEEE Engineering in Medicine and Biology Society*, 2012.

7. Cahill, B. P., "Optimization of an impedance sensor for droplet-based microfluidic systems," *Smart Sensors, Actuators, and MEMS V*, Apr 2011.

8. Ebrahimi, A., and M. A. Alam, "Droplet-based non-faradaic impedance sensors for assessment of susceptibility of escherichia coli to ampicillin in 60 min," *Biomedical Microdevices*, Vol. 19, Dec 2017.

9. Brown, M. A., Z. Abbas, A. Kleibert, R. G. Green, A. Goel, S. May, and T. M. Squires, "Determination of surface potential and electrical double-layer structure at the aqueous electrolyte-nanoparticle interface," *Physical Review X*, Vol. 6, no. 1, 2016.

10. Stojek, Z., "The electrical double layer and its structure," *Electroanalytical Methods*, p. 3–9, 2009.

11. Yang, Y., and Tsouris, *Electrical Double Layer Formation*, USA: Dekker Encyclopedia of Nanoscience and Nanotechnology, Third Edition, 2014.

12. López-García, J., J. Horno, and C. Grosse, "Differential capacitance of the diffuse double layer at electrode-electrolyte interfaces considering ions as dielectric spheres: Part i. binary electrolyte solutions," *Journal of Colloid and Interface Science*, Vol. 496, p. 531–539, 2017.

13. Holze, R., "Book review: Electrochemical methods. fundamentals and applications (2nd edition) by allen j. bard and larry r. faulkner," Vol. 41, no. 4, pp. 1–18,534–580, 2002.

14. Cortina, M., M. Esplandiu, S. Alegret, and M. D. Valle, "Urea impedimetric biosensor based on polymer degradation onto interdigitated electrodes," *Sensors and Actuators B: Chemical*, Vol. 118, no. 1-2, p. 84–89, 2006.

15. Keighley, S. D., P. Li, P. Estrela, and P. Migliorato, "Optimization of dna immobilization on gold electrodes for label-free detection by electrochemical impedance spectroscopy," *Biosensors and Bioelectronics*, Vol. 23, no. 8, p. 1291–1297, 2008.

16. "Measurements, instrumentation and sensors," *Measurement, Instrumentation, and Sensors Handbook, Second Edition*, p. 1926–1950, 2014.

17. Liang, Y., J. Huang, P. Zang, J. Kim, and W. Hu, "Molecular layer deposition of aptes on silicon nanowire biosensors: Surface characterization, stability and ph response," *Applied Surface Science*, Vol. 322, p. 202–208, 2014.

18. Vandenplas, Y., "Why monitor the ph and/or impedance in the esophagus?," *Paediatric Respiratory Reviews*, Vol. 12, 2011.

19. Fujiwara, Y., Y. Kohata, K. Nakahara, T. Tanigawa, H. Yamagami, M. Shiba, K. Watanabe, K. Tominaga, T. Watanabe, T. Arakawa, and et al., "Characteristics of nighttime reflux assessed using multichannel intraluminal impedance ph monitoring and a portable electroencephalograph," *Diseases of the Esophagus*, Vol. 29, no. 3, p. 278–284, 2015.

20. Mermelstein, J., A. C. Mermelstein, and M. M. Chait, "Proton pump inhibitor-refractory gastroesophageal reflux disease: challenges and solutions," *Clinical and Experimental Gastroenterology*, Vol. Volume 11, p. 119–134, 2018.

21. Cho, Y. K., "How to interpret esophageal impedance ph monitoring," *Journal of Neurogastroenterology and Motility*, Vol. 16, no. 3, p. 327–330, 2010.

22. Nia, P. M., W. P. Meng, F. Lorestani, M. Mahmoudian, and Y. Alias, "Electrodeposition of copper oxide/polypyrrole/reduced graphene oxide as a nonenzymatic glucose biosensor," *Sensors and Actuators B: Chemical*, Vol. 209, p. 100–108, 2015.

23. Rajapaksha, R. D. A. A., U. Hashim, S. C. B. Gopinath, and C. A. N. Fernando, "Sensitive ph detection on gold interdigitated electrodes as an electrochemical sensor," *Microsystem Technologies*, Vol. 24, no. 4, p. 1965–1974, 2017.

24. Azmi, M., S. Nadzirah, and U. Hashim, "Electrical characterization of aluminum interdigitated electrodes for ph sensing application," *2014 IEEE Conference on Biomedical Engineering and Sciences (IECBES)*, 2014.

25. Farehanim, M. A., U. Hashim, N. Azizah, M. F. Fatin, and A. H. Azman, "Fabrication of interdigitated electrodes (ides) using basic conventional lithography for ph measurement," 2017.

26. Islam, F., M. H. Haque, S. Yadav, M. N. Islam, V. Gopalan, N.-T. Nguyen, A. K. Lam, and M. J. A. Shiddiky, "An electrochemical method for sensitive and rapid detection of fam134b protein in colon cancer samples," *Scientific Reports*, Vol. 7, Sep 2017.

27. Wang, K., "Toward separation and purification of olefins using dithiolene complexes: An electrochemical approach," *Science*, Vol. 291, p. 106–109, May 2001.

28. Chatterjee, S., and A. Chen, "Facile electrochemical approach for the effective detection of guanine," *Electrochemistry Communications*, Vol. 20, p. 29–32, 2012.

29. Driver, P., "An electrochemical approach to the characterisation of black chrome selective surfaces," *Solar Energy Materials*, Vol. 4, no. 2, p. 179–202, 1981.

30. Su, Y.-Z., Y.-C. Fu, Y.-M. Wei, J.-W. Yan, and B.-W. Mao, "The electrode/ionic liquid interface: Electric double layer and metal electrodeposition," *ChemPhysChem*, Vol. 11, no. 13, p. 2764–2778, 2010.

31. Helmholtz, H., "Ueber einige gesetze der vertheilung elektrischer ströme in körperlichen leitern mit anwendung auf die thierisch-elektrischen versuche," *Annalen der Physik und Chemie*, Vol. 165, no. 6, p. 211–233, 1853.

32. Pilon, L., H. Wang, and A. Dentremont, "Recent advances in continuum modeling of interfacial and transport phenomena in electric double layer capacitors," *Journal of the Electrochemical Society*, Vol. 162, Mar 2015.

33. Technologies, K., *Impedance Measurement Handbook, A guide to measurement technology and techniques 6th Edition*, USA: Springer, 2016. www.keysight.com.

34. Lvovich, V. F., *Impedance Spectroscopy: Applications to Electrochemical and Dielectric Phenomena 2nd Edition*, Wiley, July 2012. ISBN: 978-0-470-62778-5.